CHEMISTRY
A EUROPEAN JOURNAL

DOI: 10.1002/chem.200500198

Characterization of the Monovalent Ion Position and Hydrogen-Bond Network in Guanine Quartets by DFT Calculations of NMR Parameters

Tanja van Mourik*[a] and Andrew J. Dingley*[b]

Abstract: Conformational stability of G-quartets found in telomeric DNA quadruplex structures requires the coordination of monovalent ions. Here, an extensive Hartree–Fock and density functional theory analysis of the energetically favored position of Li^+, Na^+, and K^+ ions is presented. The calculations show that at quartet–quartet distances observed in DNA quadruplex structures (3.3 Å), the Li^+ and Na^+ ions favor positions of 0.55 and 0.95 Å outside the plane of the G-quartet, respectively. The larger K^+ ion prefers a central position between successive G-quartets. The energy barrier separating the minima in the quartet-ion-quartet model are much smaller for the Li^+ and Na^+ ions compared with the K^+ ion; this suggests that K^+ ions will not move as freely through the central channel of the DNA quadruplex. Spin–spin coupling constants and isotropic chemical shifts in G-quartets extracted from crystal structures of K^+- and Na^+-coordinated DNA quadruplexes were calculated with B3LYP/6-311G(d). The results show that the sizes of the *trans*-hydrogen-bond couplings are influenced primarily by the hydrogen bond geometry and only slightly by the presence of the ion. The calculations show that the R_{N2N7} distance of the N2-H2···N7 hydrogen bond is characterized by strong correlations to both the chemical shifts of the donor group atoms and the $^{h2}J_{N2N7}$ couplings. In contrast, weaker correlations between the $^{h3}J_{N1C6'}$ couplings and single geometric factors related to the N1-H1···O6=C6 hydrogen bond are observed. As such, deriving geometric information on the hydrogen bond through the use of *trans*-hydrogen-bond couplings and chemical shifts is more complex for the N1-H1···O6=C6 hydrogen bond than for the N2-H2···N7 moiety. The computed *trans*-hydrogen-bond couplings are shown to correlate with the experimentally determined couplings. However, the experimental values do not show such strong geometric dependencies.

Keywords: density functional calculations · DNA structures · hydrogen bonds · monovalent ions · NMR spectroscopy

Introduction

Hydrogen bonds (H-bonds) play key roles in the formation and stabilization of biomacromolecular structures and as participants in enzymatic and chemical reactions.[1,2] Since the experimental detection of spin–spin coupling constants between nuclei on both sides of the H-bond in nucleic acids[3–14] and proteins,[15–23] the measurement of these couplings has emerged as a valuable tool to study biomolecular structure and function. Such electron-mediated scalar couplings identify H-bonding partners, and thus in favorable cases, the H-bond network in biomacromolecules can be established directly via a single NMR experiment. Several reports have shown that *trans*-H-bond scalar couplings yield quantitative information on H-bond geometries due to their dependence on the overlap of the donor and acceptor orbitals.[3,17,24,25] Changes in the magnitude of the coupling constants have been used to yield information on changes in H-

[a] Dr. T. van Mourik
Department of Chemistry, University College London
20 Gordon Street, London WC1H 0AJ (UK)
Fax: (+44) 207-679-7463
E-mail: t.vanmourik@ucl.ac.uk

[b] Dr. A. J. Dingley
Department of Biochemistry and Molecular Biology
University College London, Gower Street, London WC1E 6BT (UK)
Fax: (+44) 207-679-7193
E-mail: dingley@biochem.ucl.ac.uk

Supporting information for this article is available on the WWW under http://www.chemeurj.org/ or from the author: Tables S1–S5 are computed chemical shift and scalar coupling data for the various G-quartet structures. Figures S1–S3 show correlations between NMR parameters and geometric properties of the N1-H1···O6=C6 and N2-H2···N7 H-bond moieties in G-quartets. Figure S4 shows the R_{N2N7} distance as a function of the deviation of the proton from the hydrogen bond center. The Cartesian coordinates of the optimized G-quartet structures are provided.

bond geometry when biomacromolecules experience different physicochemical environments.[26–31]

Computational studies by using density functional theory (DFT) and ab initio molecular orbital methods have reproduced the trends, but not necessarily the magnitude, of the measured *trans*-H-bond couplings and donor and acceptor chemical shifts in nucleic acids[4,13,32] and proteins.[33–37] Spin–spin couplings are recognized to be one of the most difficult molecular observables to calculate, and increasing the size of the basis sets has not led to the calculated couplings matching the experimental values.[38] Most of these studies have relied solely on calculating the dominant contribution of the Fermi contact (FC) term to the overall coupling constant, and have neglected the diamagnetic spin-orbit, the paramagnetic spin-orbit, and the spin-dipole terms. Only a few recent studies, examining the H-bonds in the protein ubiquitin[39] and model peptides[40] have considered the influence of all four Ramsey[41] terms to the size of the *trans*-H-bond scalar couplings.

DNA quadruplexes that form from tandem repeats of short guanine-rich sequences found in telomeres are recognized to play important biological roles, interact with a number of proteins, and may be potential therapeutic targets against cancer.[42,43] The guanine quartet (G-quartet) motif observed in quadruplexes is characterized by four in-plane guanine bases hydrogen bonding together in a cyclic arrangement. The formation of G-quartets is crucially dependent on the interaction of monovalent cations with the guanine O6 atoms, and the type of ion present influences the stability and conformation of the quadruplexes. The location of the monovalent ions is different between the sodium/lithium and potassium quadruplex structures. The observed differences in the coordination positions of the K^+ and Na^+ or Li^+ ions are considered to be due to the different ionic radii of the ions.[44,45] The smaller Na^+/Li^+ ion is capable of residing within the plane of a G-quartet, whereas the larger K^+ ions bind between two G-quartets. Further, the Na^+ ion is less constrained by steric clashes than K^+ and can occupy a range of positions that reduce electrostatic repulsion between the adjacent ions. Experimental,[46] molecular dynamics,[47] and DFT[48–52] studies have examined the influence and preference of monovalent cations to the energetic stability of G-quartets. The results revealed that the K^+ ion rather than the Na^+ ion is preferred.[46,53] Apparently, the preference of K^+ over Na^+ is primarily due to the greater cost of Na^+ dehydration with respect to K^+, whereas the intrinsic free energy of Na^+ binding by G-quartets is more favorable than that of K^+.[46,49]

Two-bond ($^{h2}J_{NN}$) and three-bond ($^{h3}J_{NC'}$) *trans*-H-bond couplings have been measured for the N-H···N and N-H···O=C H-bond moieties in the sodium-bound Oxy-1.5 DNA quadruplex which is formed by a C_2-symmetric dimer of the oligonucleotide $d(G_4T_4G_4)$.[54] The Oxy-1.5 quadruplex contains the repeat sequence $d(T_4G_4)$ found in the protozoan *Oxytricha nova* telomeres. The sodium and potassium Oxy-1.5 quadruplexes possess the same structural topology, where the 16 guanine bases of the two monomers build a central core of four stacked hydrogen-bonded G-quartets and the thymines of each monomer form ordered loops connecting diagonally opposed corners of the bottom and top G-quartets. The detected *trans*-H-bond couplings verify the G·G Hoogsteen hydrogen bond network found in the NMR[55–57] and crystal structures[58,59] of the Oxy-1.5 DNA quadruplexes.

Here, we report the use of quantum chemistry calculations to characterise the H-bond network in G-quartets of the Na^+-, and K^+-bound Oxy-1.5 DNA quadruplex and in coplanar C_{4h} and S_4 symmetric G-quartet structures with and without ion coordination. We compute $^{h2}J_{N2N7}$ and $^{h3}J_{N1C6'}$ couplings and the isotropic chemical shifts of the nuclei involved in the N-H···N and N-H···O=C H-bond moieties for G-quartets in the K^+ and Na^+ coordinated Oxy-1.5 DNA quadruplexes and the C_{4h} symmetric structures. The results show that the magnitudes of the *trans*-H-bond scalar couplings are influenced primarily by geometric factors and only slightly (~4%) by the presence of the ions. Calculations are performed to examine the influence of Na^+, Li^+ and K^+ ions on the stability and conformation of the G-quartets. The results illustrate that at quartet–quartet distances observed in the crystal structures, the smaller Na^+/Li^+ ions show two shallow minima located just outside the plane of the G-quartet, whereas the larger K^+ has a single minimum centered between two quartets. At larger quartet–quartet distances the energy barrier between the two optimal positions for the Na^+/Li^+ ions increases, and the ions converge to a position coplanar with the G-quartet. The results show that the smaller Na^+/Li^+ ions have rather low energy barriers that under physiological conditions are most likely overcome by vibrational and thermodynamic effects. Consequently the movement of these ions through the central pore of the DNA quadruplex is presumably energetically unimpeded. In contrast, K^+ ion G-quartet models show much larger energy barriers for the movement of the ion through the central cavity of the G-quartets, indicating that the K^+ ions will not move as freely through the central channel of the DNA quadruplex.

Computational Methods

Optimization of the structure of the guanine quartet: The structure of the guanine quartet (G-quartet) at C_{4h} and S_4 symmetry was fully optimized by using NWChem,[60] with density functional theory (DFT) by using the B3LYP[61–63] and B97[64] functionals employing basis sets ranging from 6-31G(d) to 6-311++G(d,p). Similar calculations using Gaussian 03[65] failed to converge or converged to an alternative structure containing bifurcated hydrogen bonds, whereas using NWChem both the Hoogsteen H-bonded structure observed in crystallographic and NMR studies,[56–59] as well as the bifurcated structure could be optimized. The convergence problems experienced with Gaussian 03 may have arisen from the larger threshold for removal of linear dependencies (see below). The "fine" integration procedure was used for the evaluation of the exchange-correlation contribution to the density functional, except for the calculations on the S_4-symmetric structures, which used the "xfine" integration grid.

Calculation of monovalent ion position in G-quartet: The calculations on the G-quartet/metal ion complexes were performed with Gaussian 03.[65] Structures of the tetrad with a Li^+, Na^+ and K^+ ion were optimized at the B3LYP/6-31+G(d) level of theory, using Gaussian's "ultrafine" integration grid. The interaction energy between the monovalent ion and the G-quartet was computed employing the counterpoise procedure[66] to correct for basis set superposition error (BSSE):

$$\Delta E = E_{G4-M^+}^{\{G4-M^+\}}(R,r) - E_{G4}^{\{G4-M^+\}}(R,r) - E_{M^+}^{\{G4-M^+\}}(R,r) + \Delta U_{G4}^{def} \quad (1)$$

R symbolizes the intermolecular geometrical parameters and r denotes the intramolecular geometry of the G-quartet. The subscripts indicate the molecular system (G4 represents G-quartet, whereas M^+ represents metal ion), whereas the superscripts indicate whether the energy calculation was done in the monomer {G4} or dimer {G4-M^+} basis set. The last term is the G4 deformation energy (ΔU),[67] which was calculated as the energy difference between G4 fixed at the geometry it adopts in the complex (r), and G4 at its equilibrium geometry r_e (i.e., fully optimized):

$$\Delta U_{G_4}^{\mathrm{def}} = E_{G_4}^{\{G4\}}(r) - E_{G_4}^{\{G4\}}(r_e) \quad (2)$$

The first three terms in Equation (1) were computed with the Gaussian 03s counterpoise option. This option ensured that the proper integration grid points were used for the ghost atoms. Care had to be taken with the computation of the deformation energy [Eq. (2)]: Both NWChem and Gaussian 03 encountered near-linear dependencies when employing basis sets with diffuse functions, which was solved by removing the eigenvectors belonging to the smallest eigenvalues. However, NWChem and Gaussian 03 have slightly different thresholds for removal of these linear dependencies, and thus, the resulting basis sets are different sizes. For example, in B3LYP/6-31+G(d) calculations on the C_{4h} symmetric G-quartet, NWChem eliminates eight basis functions, whereas Gaussian 03 eliminates no functions. In general, calculations performed with Gaussian 03 eliminated fewer functions compared with NWChem. As explained in the previous section, $E_{G_4}^{\{G4\}}(r_e)$ was computed with NWChem. Consequently, to retain proper counterpoise $E_{G_4}^{\{G4\}}(r)$ was also calculated with NWChem.

HF/6-31G(d), B3LYP/6-311G(d,p), and B3LYP/6-311+G(d,p) single-point calculations were performed on the G4-Li^+-G4 system, whereas HF/6-31G(d) single-point calculations were performed for the G4-M^+-G4 model where M^+ represents either Na^+ and K^+ and for the G4-M^+-G4-M^+ model with M^+ representing all three monovalent ions. For the G4-M^+-G4 model the distance between the G-quartet planes was kept fixed at a range of distances, and the metal ion was placed at specific positions on the line connecting the midpoints of the G-quartet moieties. The G-quartet structures were kept rigid at their C_{4h}-symmetric geometries optimized with B3LYP/6-311++G(d,p) or the C_{4h}-symmetric G-quartet structure optimized in the presence of a monovalent ion with HF/6-31G(d). For the G4-M^+-G4-M^+ model, the quartet–quartet and ion–ion distances were fixed at 3.3 Å, and the two moieties were moved relative to each other.

Calculation of NMR properties: NMR chemical shifts and spin–spin coupling constants were computed at the DFT/B3LYP level with the 6-311G(d) basis set using Gaussian 03. This basis set was found to yield intra-base spin–spin couplings for guanine very close to those computed using larger basis sets such as 6-311++G(d,p) (see Supporting Information). Polarization functions on hydrogen atoms and diffuse functions appear to have little influence on the computed couplings. In contrast, the use of a triple-zeta basis set for the valence orbitals generally improves the agreement between the experimental and calculated couplings. For example, for the $^1J_{N1H1}$ coupling the discrepancy with the experimental value decreases from 13 to 4 Hz when the basis set is increased from 6-31+G(d) to 6-311+G(d) (see Supporting Information). We did not consider the basis set dependence of the inter-base spin–spin coupling constants. However, a recent study on the basis set dependence of $^{h3}J_{NC'}$ couplings[68] showed that these couplings are not as sensitive to the size of the basis set as some other couplings previously studied.[38] Spin–spin coupling constants were computed as the sum of the four Ramsey terms[41] (i.e., Fermi contact, spin-dipolar, paramagnetic spin-orbit and diamagnetic spin orbit terms). We computed the NMR properties for the C_{4h}-symmetric quartets optimized with B3LYP/6-311++G(d,p), and for the same optimized G-quartets with monovalent ions placed coplanar in the central cavity without subsequent reoptimization. In addition, we computed the NMR parameters for C_{4h}-symmetric G-quartets optimized with B3LYP/6-31+G(d) in the presence of a Na^+ or K^+ ion, and for G-quartets taken from the X-ray crystal structures of the K^+- (PDB accession number 1JPQ) and Na^+-loaded (PDB accession number 1JB7) DNA quadruplexes. For the inner and outer G-quartets extracted from the crystal structures, the positions of the hydrogen atoms were optimized with B3LYP/6-31G(d) using NWChem.

The shielding tensors were computed using the gauge-independent atomic orbital (GIAO) method.[69,70] The ^1H, ^{13}C and ^{15}N NMR chemical shifts reported in this study are isotropic values, indirectly referenced to tetramethylsilane (TMS), CH_4, and liquid ammonia. The structures of CH_4 and NH_3 were first optimized at the B3LYP/6-311++G(d,p) level of theory and the shielding tensors were computed with B3LYP/6-311G(d). The TMS (^1H) magnetic shielding (32.1 ppm) was obtained from the calculated shielding of gas-phase CH_4 and the known experimental difference (0.13 ppm) between gas-phase CH_4 and TMS.[71] The ^{13}C magnetic shielding (190.2 ppm) was calculated from gas-phase CH_4. The liquid NH_3 (^{15}N) magnetic shielding (252.9 ppm) was obtained from the calculated shielding of gas-phase NH_3 and the experimental difference between gas-phase NH_3 and liquid CH_3NO_2 (399.3 ppm)[72,73] and the experimental difference between liquid NH_3 and liquid CH_3NO_2 (381.9 ppm).[74]

Results and Discussion

DFT calculated geometries of guanine quartets: The G-quartet structure was optimized at both C_{4h} and S_4 symmetries. Two different C_{4h}-symmetric G-quartet structures were calculated. In one structure the guanine bases are linked by Hoogsteen G·G base pair H-bonds (Figure 1b), whereas the

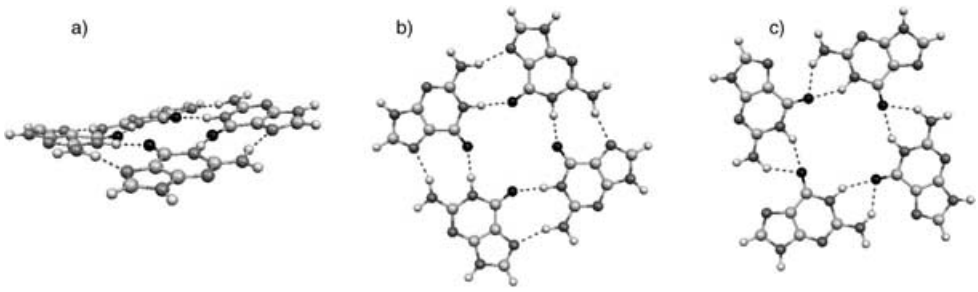

Figure 1. Structures of the S_4 and planar C_{4h} G-quartets optimized with DFT in the absence of monovalent ions. The S_4 structure depicts Hoogsteen G·G base pair H-bonds (a), whereas both Hoogsteen G·G base pairing (b) and bifurcated N-H···O H-bond (c) structures are calculated for the C_{4h} G-quartet.

second structure contains bifurcated N-H···O H-bonds (Figure 1c). In contrast, only the G·G Hoogsteen base-paired S_4-symmetric G-quartet structure was calculated (Figure 1a). The S_4-and C_{4h}-symmetric structures are essentially iso-energetic (the S_4 structure is 0.43 kJ mol^{-1} more stable at the B3LYP/6-311++G(d,p) level) at this level of theory, in agreement with previous results by Meyer et al.[51] The S_4-symmetric non-planar G-quartet is a true minimum on the B3LYP potential energy surface,[51] whereas the existence of imaginary frequencies indicates that the two C_{4h}-symmetric structures are transition states. In variance with the results of Meyer et al.,[51] which showed four imaginary frequencies for the C_{4h}-symmetric structures optimized with B3LYP/DZVP, we find only one imaginary frequency using B3LYP/6-311G(d,p); this indicates that the C_{4h}-symmetric structures are first-order transition states at the B3LYP/6-311G(d,p) level of theory.

The calculated structure of the Hoogsteen C_{4h}-symmetric G·G base-paired G-quartet is in agreement with crystal structure data[58,59] and NMR results examining the H-bond network of the oligonucleotide d($G_4T_4G_4$) which dimerizes to form a C_2-symmetric quadruplex with Hoogsteen G·G base-pairs.[57] The bifurcated H-bonded G-quartet is similar to the structure found previously by HF and B3LYP calculations on the guanine[48,52] and isoguanine[75] quartet. The Hoogsteen G·G base paired and the bifurcated H-bonded G-quartet are essentially iso-energetic in the absence of a monovalent ion (Table 1). As previously observed,[52] the relative stability of the two G-quartet structures is dependent on the level of theory applied. Using B3LYP with the 6-31G(d) and 6-311G(d,p) basis sets, the Hoogsteen G·G base-paired quartet is favored over the bifurcated H-bond G-quartet structure. The inclusion of diffuse functions, which has previously been reported to be important for calculating relative energies by DFT,[76] shifts the energy term to favor the bifurcated G-quartet structure. The use of a larger basis set with diffuse functions favors the bifurcated structure, however the energy difference (0.06 kJ mol^{-1}) is negligible. In contrast, using the largest basis set (6-311++G(d,p)) with a different functional (B97) gave a ΔE value that favors the Hoogsteen G·G base-paired quartet. Thus, electronic structure calculations do not unequivocally predict whether the bifurcated or the Hoogsteen G·G base-paired quartet is the preferred structure. An Atoms-in-Molecules (AIM) study[50] showed that the H-bonds are weaker in the bifurcated arrangement than in the Hoogsteen G·G base-paired quartet, indicating that the greater stability (at some levels of theory) of the bifurcated quartet structure compared to the Hoogsteen G·G base-paired quartet likely stems from decreased repulsion of the O6 atoms (which are further apart in the bifurcated structure), rather than from a more efficient hydrogen-bonding network. This advantage of the bifurcated arrangement is non-existent in a metal-containing quartet, providing a possible explanation for the observation that the addition of a monovalent ion to the bifurcated structure induces the formation of Hoogsteen G·G based-paired structure.[49] As metal-containing G-quartets do not seem to adopt the bifurcated structure, a result which is in agreement with experimental data that show only the Hoogsteen G·G base-paired geometric arrangement of the G-quartets, we have not considered the bifurcated structure any further in this study.

Table 1. Relative stability [kJ mol^{-1}] of the C_{4h}-symmetric bifurcated H-bonded G-quartet complex with respect to the Hoogsteen G·G H-bonded complex.

Level of theory	ΔE [kJ mol^{-1}][a]
B3LYP/6-31G(d)	2.51
B3LYP/6-311G(d,p)	1.74
B3LYP/6-31+G(d)	−2.72
B3LYP/6-31++G(d,p)	−1.84
B3LYP/6-311++G(d,p)	−0.06
B97/6-311++G(d,p)	1.12

[a] Positive ΔE values denote that the Hoogsteen G·G H-bonded G-quartet structure is more stable than the bifurcated H-bonded structure.

C_{4h}-symmetric G-quartet structures optimized with a monovalent ion positioned in the middle of the G-quartet (Figure 2a) were observed to be not true minima as indicated by the existence of imaginary frequencies (Table 2). The minimum-energy structure for the K^+ G-quartet is the C_4-symmetric geometry in which the G-quartet surface forms a convex conformation with the apex positioned directly below the K^+ ion (Figure 2b). This indicates that the K^+ ion prefers to be positioned non-coplanar to the G-quartet. The monovalent ion is located 1.57 Å above the plane of the O6 atoms (taken as the average of all guanine atoms). The K^+-bound C_{4h}-symmetric structure has one imaginary frequency, which indicates that this conformation is a transition state. The transition state links the equivalent C_4-symmetric

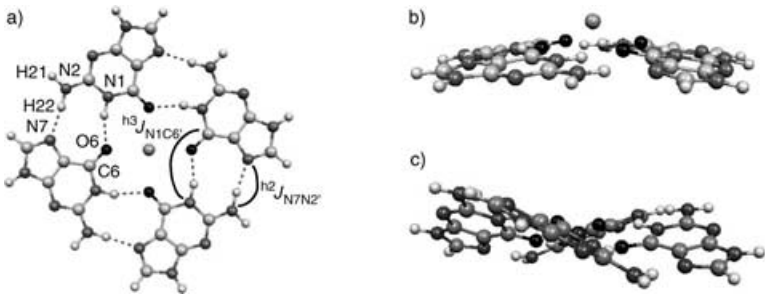

Figure 2. Structures of the Na^+- and K^+-bound G-quartets optimized using B3LYP/6-31+G(d). a) C_{4h} G-quartet with Na^+ coordinated. The overall structure of the Li^+- and K^+-bound quartets are similar with O6–O6 distances of 4.33 and 5.13 Å, respectively. Atoms involved in the two H-bonding regions of the G-quartet and relevant *trans*-H-bond coupling connectivities are indicated. b) C_4 G-quartet loaded with a K^+ ion. The ion is positioned 1.57 Å above the plane of the O6 atoms (taken as the average of all guanine atoms). This structure does not exist for the other two G-quartet species. c) S_4 G-quartet structure with Li^+ coordinated.

Table 2. Computed interaction energies [kJ mol^{-1}] between the G-quartet and the monovalent ions.

System	Sym.	Method	Basis set	D_e	Freq.[a]
G4-K$^+$	C_4	HF	6-31G(d)	–	0
	C_4	B3LYP	6-31+G(d)	−313.9	–
	C_{4h}	B3LYP	6-31+G(d)	−296.6	1
G4-Li$^+$	S_4	HF	6-31G(d)	–	4
	C_{4h}	HF	6-31G(d)	–	0
	S_4	B3LYP	6-31+G(d)	−516.7	–
	C_{4h}	B3LYP	6-31+G(d)	−507.0	–
G4-Na$^+$	C_{4h}	HF	6-31G(d)	–	2
	C_{4h}	B3LYP	6-31+G(d)	−430.4	–

[a] Number of imaginary frequencies.

minima that have the K$^+$ ion positioned on opposite sites of the G-quartet. The C_4-symmetric structure is 17 kJ mol^{-1} more stable than the C_{4h}-symmetric structure (at the B3LYP/6-31+G(d) level of theory). This value represents the energy barrier the K$^+$ ion has to surmount to pass through the G-quartet from one side to the other. The C_{4h}-symmetric Li$^+$ and Na$^+$ containing G-quartets are higher-order saddle points, as indicated by the existence of more than one imaginary frequency (Table 2). Consequently, these structures do not simply connect two minima. This implies that the Li$^+$ and Na$^+$ G-quartet potential energy landscapes are more complex than that of the G-quartet coordinated with a K$^+$ ion.

The minimum for the Li$^+$ G-quartet is the S_4-symmetric structure (Figure 2c), whereas no local minimum for the K$^+$-bound S_4-symmetric G-quartet exists.[51] The Na$^+$ S_4-symmetric G-quartet structure optimized to the C_{4h}-symmetric structure. In the S_4-symmetric Li$^+$ G-quartet, the guanine bases are strongly twisted relative to each other and the G-quartet is crudely reminiscent of a four-blade propeller. The S_4-symmetric structure allows optimal interaction between the monovalent ion and the O6 atoms of the guanine bases.[51] The O6–O6 distance (i.e., diagonal distance across the central cavity between two O6 atoms) has decreased from 4.33 (C_{4h}) to 4.03 Å (S_4) in the Li$^+$ G-quartet. The S_4 G-quartet structure contrasts strongly with the observed geometric near coplanar arrangement observed in the crystal structures of the DNA quadruplexes.[58,59] The observation that the G-quartet structure in DNA quadruplexes does not correspond to the most stable calculated S_4 G-quartet structure is mainly due to steric restraints from base stacking and backbone torsional restrictions in the G-quadruplex structure, which prevent individual G-quartets from shifting to an S_4-like conformation.

Characterizing the monovalent ion position in G-quartets: Figure 3a shows the relative energy curves for the three monovalent ions at different positions between two G-quartets that are fixed at 3.3 Å, which is the average distance measured in the crystal structures of the *Oxytricha nova* Na$^+$ and K$^+$ DNA quadruplex structures.[58,59] Optimization of the sandwiched quartet–K$^+$–quartet complex has been recently shown to lead to much larger inter-quartet distances.[77] The G4-Li$^+$-G4 relative energy curves were computed at the HF/6-31G(d), B3LYP/6-31G(d) and B3LYP/6-31+G(d) levels of theory (Figure 3b). The HF/6-31G(d) and B3LYP/6-31G(d) results are essentially identical, whereas the B3LYP/6-31+G(d) curve is only slightly different. As it is too computationally expensive to calculate the large number of points required to generate all relative energy curves with B3LYP/6-31+G(d), all subsequent calculations on the G4-M$^+$-G4 and G4-M$^+$-G4-M$^+$ model systems were performed using HF/6-31G(d). The energy profiles show that the K$^+$, Na$^+$ and Li$^+$ ions prefer to be located between two G-quartets. The energy rises much more steeply when the K$^+$ ion position moves out of the middle as compared to the other two ions. The preference of K$^+$ for the central location between the two G-quartets is generally rationalized by its larger size as compared to Na$^+$ and Li$^+$, which is believed to prevent the K$^+$ ion from occupying a position within the G-quartet plane. However, our calculations indicate that the preference of K$^+$ for the central location is not just a result of the monovalent ion's size. In our model system, the central cavity of the G-quartets is sufficiently large to accommodate a K$^+$ ion, as indicated by the contraction of the G-quartet by the presence of a K$^+$ ion (see below). Even when using a G-quartet geometry that is optimal for K$^+$ coordination, as in the potential energy profiles in Figure 3b, the K$^+$ ion still strongly prefers a position in the middle between two G-quartets. Figure 3a shows that the Na$^+$ and Li$^+$ ions also prefer a position between the G-quartets. However, unlike the K$^+$ ion results that show one deep minimum, the potential energy curves for Li$^+$ and Na$^+$ show two shallow minima located at 0.55 and 0.95 Å, respectively, from the center of a G-quartet.

For the calculations on the G4-M$^+$-G4 and the G4-M$^+$-G4-M$^+$ model systems, the G-quartet structures were kept rigid at their C_{4h}-symmetric G4 geometries optimized without the presence of an ion using B3LYP/6-311++G(d,p). This G-quartet structure has an O6–O6 (diagonal) separation of 5.15 Å. Optimizing the C_{4h}-symmetric G4-M$^+$ structures in the presence of the ions using the same level of theory (i.e., HF/6-31G(d)) as used to generate the energy profiles yields O6-O6 distances of 4.34 (Li$^+$), 4.66 (Na$^+$) and 5.19 Å (K$^+$). The O6–O6 distance in the isolated G-quartet structure optimized with HF/6-31G(d) was calculated as 5.99 Å. As such, the monovalent ion clearly causes contraction of the G-quartet. Although at shorter G4-M$^+$ distances the HF/6-31G(d) G-quartet geometry optimized in the presence of the ion would be a better choice for generating the energy curves, at larger distances a more suitable G-quartet geometry would be the HF/6-31G(d) structure optimized without the ion. As a compromise, the B3LYP/6-311++G(d,p) structure we have used gives an O6–O6 separation intermediate between those observed in the HF/6-31G(d) G-quartet structures optimized with and without the ion. Figure 3b shows that using the G-quartet structure resulting from HF/6-31G(d) geometry optimization in the presence of the ion changes the G4-Na$^+$-G4 and G4-K$^+$-G4 curves negligibly. The effect is largest for G4-Li$^+$-G4, in correspondence with the larger change in O6–O6 separation

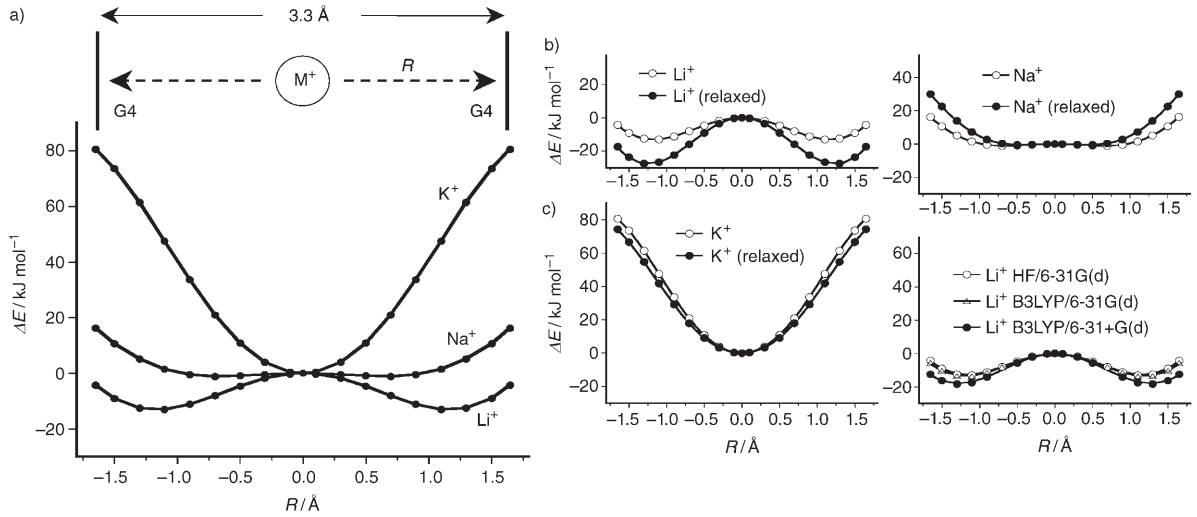

Figure 3. Relative energy curves for the three monovalent ions at different positions between two G-quartets that were fixed at the average distance measured in the crystal structures of the *Oxytricha nova* Na^+ and K^+ DNA quadruplex structures.[58,59] The energy curves were normalized by subtracting the energy at $R=0$ Å from all energy points. The x-axis coordinate R represents the distance of the ion from the center between the two quartets. a) Relative energy curves computed with HF/6-31G(d). The G-quartet structures were fixed at the B3LYP/6-311++G(d,p) optimized geometry. b) The potential energy profiles labeled relaxed were derived from G-quartet geometries optimized using HF/6-31G(d) in the presence of the ion, whereas all other curves were computed with the B3LYP/6-311++G(d,p) optimized G-quartet geometry. All energy points in the plots were computed with HF/6-31G(d), except for the lower right plot where different levels of theory were used (see Figure).

(0.81 Å). However, for the G4-Li^+-G4 system the different G-quartet structures (i.e., HF/6-31G(d) optimized with ion versus B3LYP/6-311++G(d,p) without ion) does not change the potential energy curve qualitatively.

At quartet–quartet distances shorter than 3.3 Å, the double-minimum potential curve converges towards a single minimum at $R=0.0$ Å. At a quartet–quartet distance of 3.0 Å the distance from one of the G-quartets to the optimal position of the Na^+ ion, R_{opt}(G4-Na^+), is equal to 1.5 Å (Figure 4b). This shows that the Na^+ ion favors a position equidistant from the two G-quartets. Figure 4a shows that in the G4-Na^+-G4 system the barrier separating the two minima becomes larger with increasing quartet–quartet distance. The R_{opt}(G4-Na^+) distance decreases with increasing quartet–quartet distance. At quartet-quartet distances beyond ~7.0 Å, at which point the influence of the second G-quartet has become negligible, the Na^+ ion prefers to be located in the central cavity of the G-quartet (i.e., R_{opt}(G4-Na^+) = 0 Å). This is also the optimal position for a Na^+ ion interacting with a single G-quartet. Figure 4c shows that it is unfavorable for Na^+ to

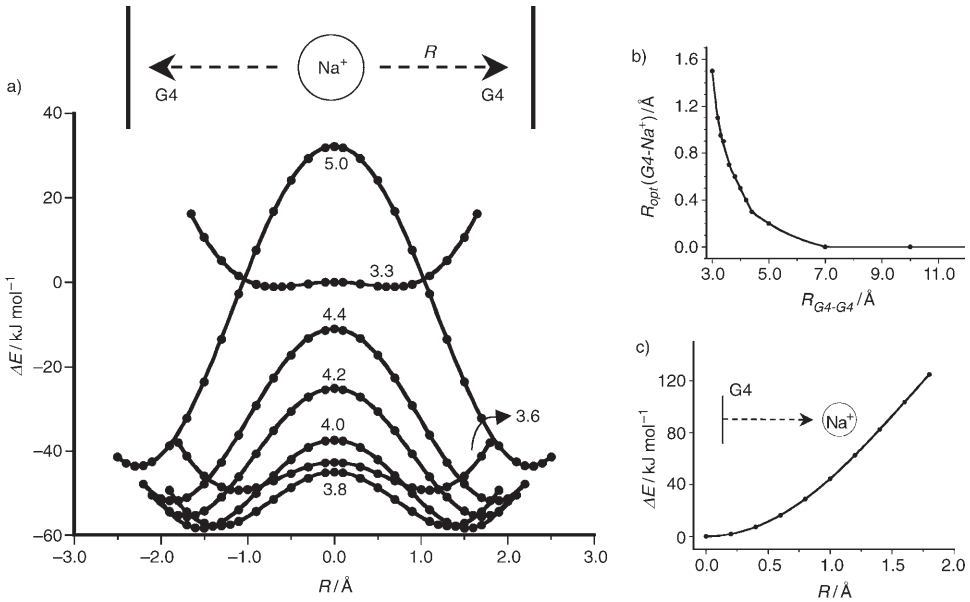

Figure 4. a) Relative energy curves for G4-Na^+-G4 at different G4-G4 distances. All points were calculated with HF/6-31G(d). The G-quartet structures were fixed at the B3LYP/6-311++G(d,p) optimized geometry. The energy curves were normalized by subtracting the energy at $R=0$ Å (G4–G4 = 3.3 Å) from all energy points. The values for each curve represent the G4–G4 distance at which the data points were computed. b) The distance from the optimal position of Na^+ (i.e., minima in a) to one of the G-quartets as a function of G4–G4 distance. At G4-G4 distances beyond approximately 7 Å the Na^+ ion prefers to sit within the plane of a G-quartet. c) The relative energy curve for G4-Na^+ calculated with HF/6-31G(d) and the G-quartet optimized with B3LYP/6-311++G(d,p). The energy curves were normalized by subtracting the energy at $R=0$ Å from all energy points.

move away from its central position in the G-quartet. However, in the G4-Na^+-G4 model, the ion is not only drawn towards the central cavity position of one G-quartet, but is also attracted to the second G-quartet. Consequently, these two competing forces result in an optimal Na^+ ion position outside the central cavity at a G4–G4 distance of 3.3 Å (Figure 3a).

The preferred central position of the K^+ ion at a quartet–quartet separation of 3.3 Å could be due to the ion being either attracted to or repelled by both G-quartets equally. Figure 5a illustrates that when the distance between the two G-quartets is increased to 5 Å and beyond a single K^+ ion will find two optimal positions located closer to the G-quartets. This observation shows that in the absence of additional ions, the single K^+ ion is not repelled by, but attracted to both G-quartets equally. Unlike the results for the Na^+ ion, the optimal position of the K^+ ion does not converge to a position coplanar with one of the G-quartets when the G4–G4 separation is increased, but converges to a distance of 0.8 Å from the G-quartet (Figure 5b). This is also the optimal position for a K^+ ion interacting with a single G-quartet (Figure 5c). For both G4-Na^+-G4 (Figure 4a) and G4-K^+-G4 (Figure 5a), the lowest energy minimum is reached for a quartet–quartet distance of 4.0 Å. However, whereas Na^+ prefers to be close to one of the G-quartets at this separation, the optimal position for K^+ is equidistant from the two G-quartets.

To provide a potentially more realistic model for the DNA quadruplexes we modified our single ion model to include an additional monovalent ion. Figure 6 shows the relative energy profiles when both ions move simultaneously away from the coplanar position in the G-quartets. The Na^+ and Li^+ ions show a clear preference for positioning in the center of the G-quartet plane since the energy values increase steeply as the monovalent ions move out of the plane of the G-quartets. In contrast, the decrease in energy for the K^+-bound system shows that this ion favors coordination near equidistant from the two G-quartets. In general, the results are in agreement with experimental data that have shown that the smaller Na^+ and Li^+ ions can adopt a coplanar position, whereas the larger K^+ ions are always embedded between the G-quartets.[59]

The minimum in the potential energy curve of the K^+-containing system is located slightly before the central position between the G-quartets, whereas the crystal structure of the K^+-containing DNA quadruplex shows that the K^+ ions are located symmetrically between two G-quartet planes.[59] The off-center minimum in the K^+ curve is most likely an artifact of the G4-M^+-G4-M^+ model. The slight increase in the energy curve for the K^+ ion as it reaches the center between the two G-quartets ($R=0$ Å) is probably due to the loss of favorable interacting energy between the G-quartet and the second ion, which is not compensated by attraction with a third G-quartet. Increasing the number of G-quartets and ions in the model may shift the energy minimum for the K^+ system towards an R-value of 0 Å, whereas for the Na^+ and Li^+ energy profiles, a maximum would be expected at an equidistant between the two G-quartets. The

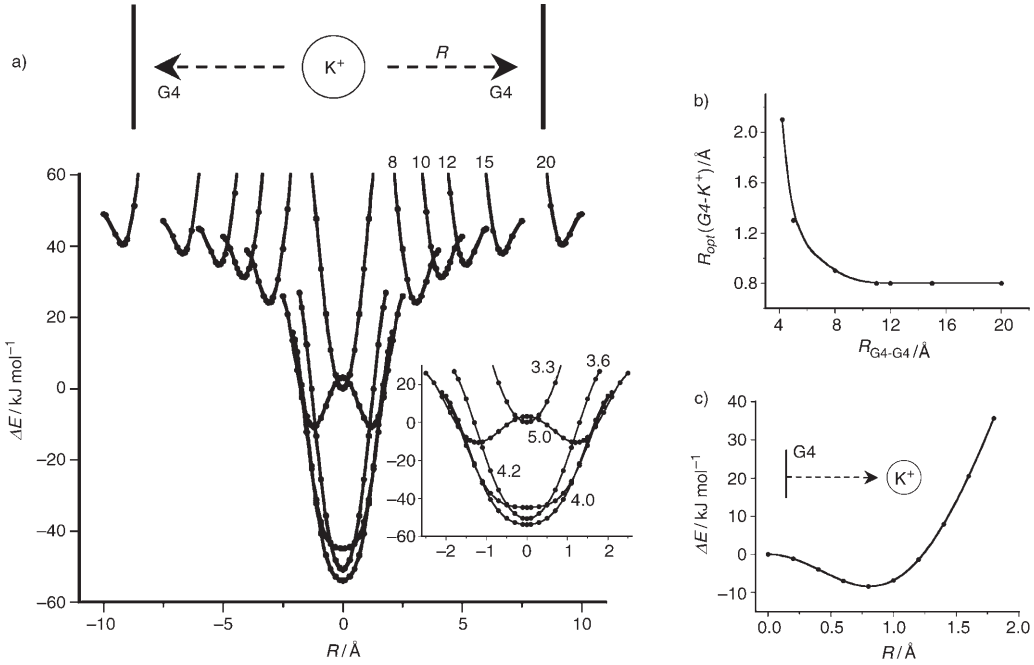

Figure 5. a) Relative energy curves for G4-K^+-G4 at different G4–G4 distances. All points were calculated with HF/6-31G(d). The G-quartet structures were fixed at the B3LYP/6-311++G(d,p) optimized geometry. The energy curves were normalized by subtracting the energy at $R=0$ Å (G4–G4 = 3.3 Å) from all energy points. The values for each curve represent the G4-G4 distance at which the data points were computed. The inset represents an expanded region of the Figure at the shorter G4–G4 distances (3.3–5.0 Å). b) The distance from the optimal position of K^+ to one of the G-quartets as a function of G4-G4 distance. At G4–G4 distances beyond approximately 10 Å the K^+ ion prefers to sit 0.8 Å outside the plane of the G-quartet. c) Relative energy curve for G4-K^+ calculated with HF/6-31G(d) and the G-quartet optimized with B3LYP/6-311++G(d,p). The energy curves were normalized by subtracting the energy at $R=0$ Å from all energy points. The minimum occurs at a distance of ~0.8 Å.

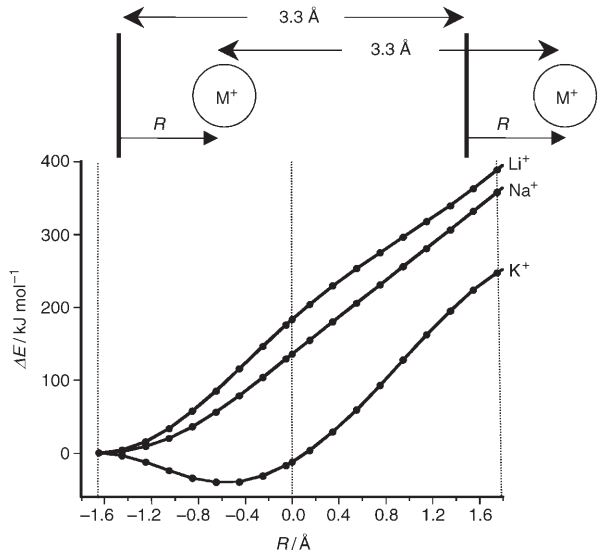

Figure 6. Relative energy curves for the G4-M$^+$-G4-M$^+$ model computed with HF/6-31G(d) and the G-quartet optimized with B3LYP/6-311++G-(d,p). Distances between the G-quartets and between the two ions were kept fixed at 3.3 Å. The energy profiles were normalized by subtracting the energy at $R=-1.65$ Å from all energy points. $R=0$ Å is defined as the mid-point position between two G-quartets.

use of a one-dimensional periodic model should more effectively describe the movement of ions through the central pore of DNA quadruplexes.

Dependence of spin–spin coupling constants on G-quartet geometry: Although the S_4-symmetric structure was found to be slightly more stable than the C_{4h}-symmetric geometry for the Li$^+$- and Na$^+$-loaded G-quartets (Table 2), the calculation of NMR properties was performed using the C_{4h}-symmetric G-quartets. This is because the conformation of the S_4-symmetric structure adopts a twisted non-coplanar geometry (especially in the presence of ions), whereas the C_{4h}-symmetric structure closely resembles the near coplanar geometry observed for the G-quartets in the crystal structures of DNA quadruplexes.[45,58] Intra- and inter-base scalar couplings were calculated for the G-quartet. In general the intra-base couplings were found to be in close agreement with experimental[78,79] and theoretical[32,80,81] values (see Supporting Information). Table 3 shows the calculated and experimental scalar couplings associated with the two H-bond moieties of the G-quartet. The $^{h3}J_{N1C6'}$ coupling for the C_{4h}-symmetric G-quartet optimized in the absence of a monovalent ion is significantly different to the experimental values with an overestimation of ~0.8 Hz (~350%). The computed $^{h2}J_{N2N7}$ coupling, however, is only slightly underestimated with an average deviation of ~1 Hz (15%). The addition of Li$^+$, Na$^+$, or K$^+$ ions (without reoptimization) does not significantly change the values of the calculated $^{h2}J_{N2N7}$ and $^{h3}J_{N1C6'}$ couplings; this indicates that the presence and type of the ion has little effect on the magnitude of the *trans*-H-bond couplings.

Reoptimization of the G-quartet structure in the presence of the Na$^+$ ion yields computed *trans*-H-bond couplings that are in closer agreement with the experimental values. This is mainly a geometric effect (see below), as removal of the Na$^+$ ion from this structure without reoptimization of the G-quartet geometry has a very small influence on the $^{h2}J_{N2N7}$ ($\Delta=0.01$ Hz) and $^{h3}J_{N1C6'}$ ($\Delta=0.04$ Hz) scalar coupling sizes. The slightly weaker absolute size of the $^{h3}J_{N1C6'}$ coupling in the presence of the ion may be due to the subtraction of electron density from the N1-H1···O6=C6 H-bond moiety when the Na$^+$ coordinates with the O6 atoms of the guanine bases. Removal of the ion presumably leads to an increase in the electronic overlap between H1 and O6 and consequently results in the observed small increase (~10%) in the size of the $|^{h3}J_{N1C6'}|$ coupling. Similarly, Sychrovský et al. attributed the observed decrease in the $^1J_{C6O6}$ coupling to charge transfer from guanine to the monovalent cation.[82] The $^1J_{N1H1}$ coupling also shows a small absolute increase in size of ~2.0 Hz when the couplings are calculated in the absence of the ion. Apparently the presence of the ion decreases the strength of the structurally proximate N1–H1 bond (Figure 2). Similar ion-dependent correlations for the scalar couplings associated with the N2-H2···N7 H-bond (i.e., $^1J_{N2H2}$ and $^{h2}J_{N2N7}$) are not observed. This is presumably due to the larger distance between the ion and the N2-H2···N7 H-bond.

Calculation of the spin–spin couplings for the G-quartet reoptimized with a co-planar K$^+$ ion does not yield *trans*-H-bond couplings in agreement with the experimental values. In the K$^+$-loaded DNA quadruplex crystal structure the K$^+$

Table 3. Spin–spin coupling constants of the C_{4h}-symmetric G-quartet (G4) and of G-quartets with a monovalent ion in the middle of the central cavity (G4-M$^+$, M = Li, Na, or K). All couplings are computed with B3LYP/6-311G(d).

	B3LYP/6-311++G(d,p) G-quartet geometry[a]				B3LYP/6-31+G(d) G4M$^+$ geometry			
	G4	G4-Li$^+$	G4-Na$^+$	G4-K$^+$	G4-Na$^+$	G4 (no Na$^+$)[b]	G4-K$^+$[c]	Experimental[d]
$^1J_{N1H1}$	−89.74[e]	−87.60	−87.46	−87.19	−88.59	−90.17	−88.63	90.21
$^1J_{N2H22}$	−88.94	−91.06	−91.03	−91.02	−89.77	−87.68	−90.78	88.05
$^1J_{N2H21}$	−97.22	−96.74	−96.72	−96.70	−94.75	−95.06	−96.76	88.05
$^{h2}J_{N2N7}$	5.82	5.87	5.88	5.88	7.66	7.67	5.22	7.06
$^{h3}J_{N1C6'}$	−1.13	−1.03	−1.04	−1.08	−0.33	−0.37	−0.59	0.22

[a] In the complexes of the G-quartet the monovalent ion is placed in the middle of the cavity of the G-quartet optimized with B3LYP/6-311++G(d,p). No re-optimization is applied. [b] G-quartet geometry taken from the B3LYP/6-31+G(d) optimized G4-Na$^+$ structure. [c] Transition state structure. [d] Average ($N=5$) $^{h2}J_{N2N7}$, $^{h3}J_{N1C6'}$, $^1J_{N2H2}$ and $^1J_{N1H1}$ values measured at 274 K for the Na$^+$-loaded Oxy-1.5 DNA quadruplex.[54] The sign of the couplings was not determined. [e] Couplings are in Hz.

ions are positioned between quartets, and thus, the coplanar K^+-quartet is not an ideal model for this system, explaining the weak correlation between the theoretical and experimental $^{h2}J_{N2N7}$ and $^{h3}J_{N1C6'}$ values. The better model to compute the $^{h2}J_{N2N7}$ and $^{h3}J_{N1C6'}$ couplings for the K^+-loaded G-quartets would be a system in which a K^+ ion is located between two G-quartets. However, such a calculation is computationally prohibitive.

Figure 7 shows the theoretical $^{h2}J_{N2N7}$ and $^{h1}J_{H2N7}$ couplings as a function of the R_{N2N7} distance. The experimental $^{h2}J_{N2N7}$ couplings taken from a previous study[54] are also plotted in Figure 7a, whereas due to amino group dynamics and the relatively small size of the $^{h1}J_{HN}$ coupling, the accurate determination of $^{h1}J_{HN}$ couplings was not possible. The scalar couplings are computed for G-quartets taken from the crystal structures of the Na^+ (PDB accession number 1JB7) and K^+ (PDB accession number 1JPQ) coordinated DNA quadruplexes, for which the hydrogen positions were optimized with B3LYP/6-31G(d). The experimental $^{h2}J_{N2N7}$ couplings are plotted at the average R_{N2N7} distance taken from the high-resolution DNA quadruplex crystal structures for each symmetry-related H-bond pair.

For each crystal structure, the H-bond geometries in the two inner and two outer quartets are not identical, and therefore 16 distinct $^{h2}J_{N2N7}$ couplings were computed (Table 4). Conversely, in the NMR experiments only eight $^{h2}J_{N2N7}$ correlations are visible since the two d($G_4T_4G_4$) monomers are symmetry related in solution. However, due to exchange broadening only five $^{h2}J_{N2N7}$ couplings have been observed in the Na^+-bound DNA quadruplex at 274 K.[54] Larger variations in R_{N2N7} are found for the outer quartets compared to the inner quartets, reflecting the lower steric constraints placed on the outer G-quartets. This variation leads to a larger range in the magnitude of the computed $^{h2}J_{N2N7}$ couplings. In addition, significant R_{N2N7} differences are observed for a particular H-bond. For example, the G12–G4*/G12*–G4 pair R_{N2N7} distances are 2.88 and 3.05 Å. Theoretical calculations for other base pair moieties considering only the Fermi contact term yielded smaller $^{h2}J_{N2N7}$ couplings.[32] These differences in $^{h2}J_{NN}$ coupling sizes are not due to H-bond R_{NN} differences since Barfield et al.[32] covered the R_{NN} range considered in the current manuscript. Additionally, the impact of the other three Ramsay terms is negligible for this particular *trans*-H-bond coupling (i.e., < 0.1 Hz). Presumably the disparity in the calculated couplings is mainly due to the different density functionals applied in each study (i.e., B3PW91 versus B3LYP). To quantify the apparent difference, a comparison of the couplings computed using B3PW91/6-311G(d,p) and B3LYP/6-311G(d,p) for the C_{4h}-symmetric G-quartet showed that B3PW91 yields smaller (~6%) $^{h2}J_{N2N7}$ and $^{1}J_{N2H2}$ couplings than B3LYP. Considering these methodological differences, the $^{h2}J_{N2N7}$ couplings are in close agreement with those published by Barfield et al.[32] The calculated $^{h2}J_{N2N7}$ couplings decrease exponentially with increasing R_{N2N7} distance. The exponential dependence on R_{N2N7} arises from the square of the overlap integrals between atomic orbitals on the donor and acceptor groups.[83] Figure 7 shows the exponential fit for the outer and inner quartets in both DNA quadruplexes, which yields the following relationship:

$$^{h2}J_{N2N7} = 2316 \exp(-1.96\, R_{N2N7}) \quad (3)$$

with a standard deviation of 0.23 Hz and $r^2 = 0.986$. The inverse of this equation yields:

$$R_{N2N7} = 3.95 - 0.51 \ln(^{h2}J_{N2N7}) \quad (4)$$

The rms difference between the R_{N2N7} distances derived from Equation (4) and the crystal structure data equals 0.017 Å. The equations only take the distance dependence of the $^{h2}J_{N2N7}$ couplings into account and ignore other geometric factors such as the N2-H2···N7 angle. Inspection of the $\sphericalangle$N2-H2···N7 versus $^{h2}J_{N2N7}$ coupling shows no apparent correlation (data not shown). The experimental $^{h2}J_{N2N7}$ coupling data shows a much weaker relation to the R_{N2N7} distance. This is due to factors such as the dynamic nature of the DNA quadruplex in solution or genuine geometric differences between the solution and crystalline states.

The computed $^{h2}J_{N2N7}$ couplings show a larger range in magnitude compared with the experimental $^{h2}J_{N2N7}$

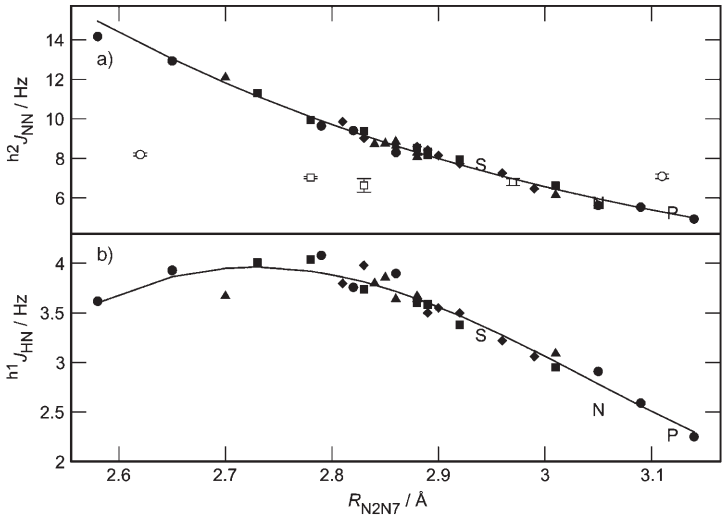

Figure 7. Calculated (filled symbols) and experimental (open symbols) a) $^{h2}J_{N2N7}$ and b) $^{h1}J_{HN}$ couplings as a function of the R_{N2N7} distance. The theoretical coupling values were calculated for G-quartet structures taken from the crystallographic data with the hydrogen atom positions optimized using B3LYP/6-31G(d). Computed data for the different G-quartets are represented by filled circles (outer quartets, Na^+ species), filled squares (inner quartet, Na^+ species), filled triangles (outer quartet, K^+ species) and filled diamonds (inner quartet, K^+ species). The experimental couplings are represented by the corresponding open symbols. These couplings are plotted at the R_{N2N7} distance obtained by averaging over the equivalent H-bonds (e.g. G1*–G9 and G1–G9*). $^{h2}J_{N2N7}$ and $^{h1}J_{HN}$ couplings calculated for the C_{4h}-symmetric G-quartet structures in the absence of an ion and in the presence of K^+ and Na^+ are represented by the symbols N, P and S, respectively. The curve in a) is the best fit exponential to the theoretical data calculated for the G-quartets taken for the crystal structures. The continuous line in b) represents a third-order polynomial fit to the data.

Table 4. Computed spin–spin coupling constants and geometric parameters related to the N2-H2···N7 H-bond in optimized G4-M^+ (M = Na, K) quartets and in G-quartets taken from the Na^+ and K^+ DNA quadruplexes with the hydrogen atom positions optimized using B3LYP/6-31G(d).

	R_{N2N7} [Å]		∢(N2H2N7) [°]		$^1J_{N2H21}$ [Hz]		$^1J_{N2H22}$ [Hz]		$^{h1}J_{H2N7}$ [Hz]		$^{h2}J_{N2N7}$ [Hz]	
	Na^+	K^+	Na^+	K^+	Na^+	K^+	Na^+	K^+	Na^+	K^+	Na^+	K^+
B3LYP/6-31+G(d) optimized C_{4h}-symmetric quartet with a monovalent ion in the middle of the cavity	2.94	3.12	174.7	166.9	−94.8	−96.8	−89.8	−90.8	3.3	2.3	7.7	5.2
outer quartet (donor guanine → acceptor guanine)												
1→9*	2.65	2.70	174.2	169.2	−88.1	−92.2	−82.1	−82.1	3.9	3.7	12.9	12.1
9*→12	3.09	2.88	177.1	178.9	−94.1	−91.3	−87.7	−86.2	2.6	3.6	5.5	8.1
12→4*	3.05	3.01	176.0	173.8	−90.1	−89.4	−83.8	−82.1	2.9	3.1	5.6	6.2
4*→1	2.79	2.86	170.7	170.9	−89.7	−91.1	−83.3	−83.9	4.1	3.8	9.7	8.6
inner quartet												
2→3*	2.78	2.89	174.6	175.6	−89.2	−94.0	−82.6	−86.1	4.0	3.5	10.0	8.4
3*→11	3.01	2.90	175.9	175.7	−94.7	−94.3	−87.0	−87.7	3.0	3.6	6.6	8.2
11→10*	2.88	2.81	171.5	174.4	−95.2	−93.8	−85.7	−86.2	3.6	3.8	8.5	9.9
10*→2	2.83	2.83	168.1	178.0	−95.2	−91.0	−85.8	−87.2	3.7	4.0	9.4	9.0
inner quartet												
3→11*	2.92	2.88	172.0	173.2	−94.1	−93.9	−85.8	−87.4	3.4	3.6	8.0	8.6
11*→10	2.89	2.96	170.9	178.8	−93.7	−94.0	−85.1	−89.4	3.6	3.2	8.4	7.3
10→2*	2.73	2.92	166.2	176.3	−93.4	−93.3	−83.8	−88.6	4.0	3.5	11.3	7.7
2*→3	2.89	2.99	170.4	176.8	−92.0	−92.6	−83.9	−89.8	3.6	3.1	8.2	6.5
outer quartet												
4→1*	2.82	2.85	167.2	172.1	−92.8	−90.5	−84.3	−83.3	3.8	3.9	9.4	8.8
1*→9	2.58	2.86	176.2	175.3	−85.5	−94.1	−81.0	−86.0	3.6	3.6	14.2	8.9
9→12*	3.14	2.88	176.3	178.0	−94.6	−93.1	−87.9	−89.3	2.3	3.7	4.9	8.3
12*→4	2.86	2.84	175.2	175.6	−90.0	−89.3	−82.3	−82.1	3.9	3.8	8.3	8.7

couplings. At shorter distances, the theoretical couplings are much larger than the experimental values, whereas at R_{N2N7} distances beyond approximately 3 Å the experimental $^{h2}J_{N2N7}$ couplings are larger. All couplings were computed in gas-phase structures at 0 K with fixed inter-nuclear distances, whereas the experimental *trans*-H-bond couplings are measured at 274 K and include influences from rovibrational averaging, environment (i.e., solvent), and inter-quartet and sugar-backbone interactions. Though it is not known how these factors influence the coupling constants, it is probable that the different experimental and theoretical conditions are responsible for the different distance dependencies observed. In proteins, the consideration of dynamical effects in the calculation of the FC term for $^{h3}J_{N1C6'}$ couplings led to an improvement in the correlation between experimental and theoretical values.[84] Future efforts that consider dynamical and solvent influences may lead to an improved correlation between the experimental and theoretical *trans*-H-bond couplings in the G-quartets.

The shortest R_{N2N7} distance is found for hydrogen bonds with the smallest difference between the N2–H2 and H2···N7 distances (see Supporting Information). This observation is in accord with a previous study,[85] which showed that the F···F and N···N distances in $[F(HF)_n]^-$ and $[CN\cdots H\cdots NC]^-$ complexes contract when the proton is shifted towards the hydrogen-bond center.

The calculated $^{h1}J_{HN}$ couplings showed a maximum value of ~4 Hz at an R_{N2N7} distance of ~2.8 Å (Table 4 and Figure 7b). At shorter and longer R_{N2N7} distances the $^{h1}J_{HN}$ couplings gradually decrease in magnitude. The decrease in the size of the $^{h1}J_{HN}$ coupling as the H-bond shortens below 2.7 Å is unexpected, whereas the weakening of the $^{h1}J_{HN}$ coupling as the H-bond increases in length is due to the reduction in the orbital overlap associated with the H-bond. Calculated $^{h1}J_{HN}$ couplings for imino groups H-bonded to aromatic acceptor nitrogen atoms showed similar trends, in which a maximum coupling size of ~3 Hz was observed at an R_{N2N7} distance of ~2.8 Å.[32] This study observed that at H-bond distances shorter than 2.6 Å the sign of the coupling was negative. According to Figure 7b, at H-bond lengths much shorter than 2.5 Å, the sign of the $^{h1}J_{HN}$ scalar coupling for the N2-H2···N7 H-bond group will also be negative. Barfield et al.[32] proposed that this decrease in the size of the $^{h1}J_{HN}$ couplings at shorter R_{N2N7} distances could be explained by symmetry considerations of the N-H···N H-bond and the associated $^{h1}J_{HN}$, $^1J_{NH}$ and $^{h2}J_{N2N7}$ couplings. They showed that as the R_{N2N7} decreases, the size of the $^{h1}J_{HN}$ coupling changes from a positive to a negative value, whereas the covalent $^1J_{NH}$ coupling decreases in size to a smaller negative value. In the symmetric H-bond arrangement where the proton is centered between the two nitrogen atoms, the $^{h1}J_{HN}$ coupling will be equal (ignoring different electronic effects from donor and acceptor groups) to the covalent $^1J_{NH}$ coupling, with both couplings having negative values. Benedict et al. have also observed a sign change for the $^1J_{FH}$ and $^1J_{NH}$ couplings when the hydrogen moves across the center of the F···F and N···N H-bond.[85] The results of the current study corroborate these previous studies and indicate that the size and sign of the $^{h1}J_{HN}$ coupling is not influenced by the chemical structure of the H-bond but primarily by the H-bond geometry.

Figure 8a shows a strong linear correlation ($r^2 = 0.98$) between the calculated isotropic chemical shift δ_H of the amino proton participating in the H-bond (^{1}H2) and the

$^{h2}J_{N2N7}$ coupling, where a downfield chemical shift corresponds to a larger $^{h2}J_{N2N7}$ value. Similar correlations have been observed between experimentally determined *trans*-H-bond couplings and isotropic chemical shifts in proteins[15,24] and in a DNA triplex.[4] The experimental and theoretical ^{1}H2 chemical shifts are very similar with theoretical calculations within 1.5 ppm of the experimental values (Table 6). In contrast, there is no clear correlation ($r^2 = 0.48$) between the isotropic chemical shift of the H-bonding ^{1}H2 and the $^{1}J_{NH}$ coupling constant for the N-H of the amino group involved in H-bonding to the acceptor N7 atom (Figure 8b). This was rather unexpected since theoretical[32] and experimental[4] results have shown a strong correlation between the imino ^{1}H isotropic chemical shift and the $^{1}J_{NH}$ coupling constant in base-paired triplets.

The calculated $^{1}J_{NH}$ couplings range between −81 to −96 Hz (Table 4) and are similar in size to previously determined $^{1}J_{NH}$ couplings in guanine bases (~91 Hz).[78] The $^{1}J_{NH}$ coupling constants for the H-bonded N-H of the amino group are larger, on average, by ~2 Hz compared with the experimental values, whereas the $^{1}J_{NH}$ couplings for the non-H-bonded N-H are smaller by ~5 Hz (Table 4). This contrasts previous theoretical results[32] that showed that H-bonded imino groups generally have smaller $|^{1}J_{NH}|$ coupling constants compared with the corresponding non-H-bonded imino groups. To investigate whether this was due to methodology differences, calculations of the spin–spin couplings in the C_{4h} symmetric G-quartet and a single guanine base (i.e., non-H-bonded) using the same functional and basis set (i.e., B3PW91/6-311G(d,p)) as used in the previous study were performed and compared with the calculations using B3LYP/6-311G(d). The calculation using B3PW91/6-311G(d,p) yielded $^{1}J_{NH}$ couplings that were

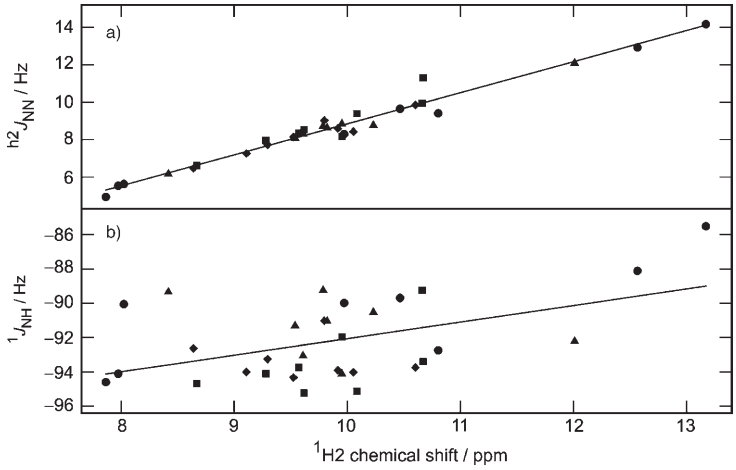

Figure 8. Correlations between a) $^{h2}J_{N2N7}$ and b) $^{1}J_{NH}$ couplings and the isotropic chemical shift of the amino proton δ_H participating in the H-bond (^{1}H2). The theoretical coupling values were calculated for G-quartet structures taken from the crystallographic data with the hydrogen atom positions optimized using B3LYP/6-31G(d). Computed data for the different G-quartets are represented by the same symbols as in Figure 7. The continuous line in a) corresponds to a linear regression of $^{h2}J_{N2N7} = (1.66\ \text{Hz ppm}^{-1})\delta_H - 7.75$ Hz ($r^2 = 0.98$). The linear regression in b) gives $r^2 = 0.48$.

Table 5. Computed spin–spin coupling constants and geometric parameters related to the N1-H1···O6=C6 H-bond in optimized G4-M$^+$ (M = Na, K) quartets and in G-quartets taken from the Na$^+$ and K$^+$ DNA quadruplexes with the hydrogen atom positions optimized using B3LYP/6-31G(d).

	R_{N1O6} [Å]		∢(H1O6C6) [°]		∢(N1H1O6) [°]		$^{1}J_{N1H1}$ [Hz]		$^{h3}J_{N1C6'}$ [Hz]	
	Na$^+$	K$^+$	Na$^+$	K$^+$	Na$^+$	K$^+$	Na$^+$	K$^+$	Na$^+$	K$^+$
B3LYP/6-31+G(d) optimized C_{4h}-symmetric quartet with a monovalent ion in the middle of the cavity	2.90	2.99	129.8	141.8	164.6	174.4	−88.59	−88.63	−0.333	−0.585
outer quartet (donor guanine → acceptor guanine)										
1→9*	2.91	2.85	121.2	127.7	159.8	167.1	−89.27	−89.79	−0.086	−0.306
9*→12	2.95	2.88	126.4	121.1	159.7	160.6	−89.86	−91.16	−0.170	−0.082
12→4*	2.95	2.91	127.6	128.6	164.6	162.5	−89.59	−88.94	−0.239	−0.287
4*→1	2.91	2.80	124.1	129.2	161.2	160.5	−89.30	−87.24	−0.167	−0.368
inner quartet										
2→3*	2.96	3.01	123.6	125.2	162.7	160.9	−89.93	−89.19	−0.122	−0.152
3*→11	2.93	2.82	128.5	127.4	161.9	160.6	−89.78	−88.56	−0.203	−0.345
11→10*	2.82	2.85	131.7	126.3	166.4	162.4	−89.03	−89.10	−0.492	−0.286
10*→2	2.86	2.84	132.8	126.2	170.6	162.5	−88.99	−92.43	−0.510	−0.307
inner quartet										
3→11*	2.91	2.90	129.8	133.2	164.6	165.3	−89.68	−90.40	−0.341	−0.519
11*→10	2.74	2.96	132.7	122.2	165.7	158.1	−88.07	−86.27	−0.718	−0.101
10→2*	2.81	2.86	133.0	131.4	172.0	162.5	−88.73	−90.56	−0.600	−0.522
2*→3	2.86	2.87	132.6	126.6	166.9	161.9	−89.41	−87.46	−0.510	−0.302
outer quartet										
4→1*	3.02	2.86	128.5	129.9	169.5	159.7	−90.00	−88.32	−0.228	−0.366
1*→9	2.85	2.81	116.4	127.2	155.6	162.3	−89.04	−91.31	0.045	−0.364
9→12*	2.93	2.85	129.5	128.5	162.2	162.4	−89.89	−89.55	−0.297	−0.423
12*→4	2.70	2.85	129.1	125.2	164.6	160.8	−87.54	−87.08	−0.583	−0.282

~5 Hz smaller compared with the same coupling calculated using B3LYP/6-311G(d). Closer examination reveals that this difference arises mainly from the Fermi contact term, and not from the other three contributing terms. In addition, both calculations show the same trends for changes in the size of the $^{1}J_{NH}$ coupling constants upon guanine base pairing in a G-quartet. Consequently, the use of different functionals and basis sets to calculate the coupling constants does not account for the discrepancy between the $^{1}J_{NH}$ trends observed for imino versus amino groups.

The computed couplings using B3LYP/6-311G(d) for the guanine monomer yielded two $^{1}J_{NH}$ couplings that are near identical in magnitude (i.e., -93 ± 0.24 Hz). In the optimized C_{4h}-symmetric guanine quartet, the calculations yielded -97 Hz for the H-bonded compared with -89 Hz for the non-H-bonded N-H moiety of the amino group. In apparent disagreement with the couplings, the H-bonded N–H distance is longer (1.0195 Å) compared to the non-H-bonded N–H distance (1.0060 Å). As the geometries of the isolated and H-bonded guanines are identical, the changes in $^{1}J_{NH}$ must be purely electronic structure effects and the contrasting trends calculated for $^{1}J_{NH}$ couplings in imino and amino groups are based on the chemical differences between these two H-bond donor groups.

Compared with the experimental values, the computed ^{15}N2 donor and ^{15}N7 acceptor isotropic chemical shifts are overestimated by approximately 20 and 40 ppm, respectively (Table 6). The theoretical ^{1}H2 isotropic chemical shifts for the amino proton involved in the N2-H2···N7 H-bond are only slightly overestimated, whereas the isotropic chemical shifts for the non-H-bonded amino proton are underestimated by ~3 ppm. The disparities between the experimental and computed chemical shifts are reasonable considering the calculations were performed for isolated G-quartets. As such, the calculations do not reflect the electronic environments produced by the intricate intra- and intermolecular interactions from solvent and other structural features of the DNA quadruplex. For example, the stacking of the G-quartets in the DNA quadruplex structure would lead to ring current effects that are not considered in the theoretical calculations. The underestimation of the ^{1}H2 chemical shift of the non-H-bonded amino proton is partly due to the absence of solvent molecules H-bonding with this free donor N–H group. In the presence of solvent, the H-bonding of this free donor group with water would lead to electron deshielding of the amino proton nucleus and a consequent ^{1}H downfield shift. Clearly DFT calculations that include explicit water molecules or water continuum models may provide information on the influences of solvent on the sizes of the *trans*-H-bond couplings and isotropic chemical shifts.

As for the $^{h2}J_{N2N7}$ couplings, the H-bond geometries in the two inner and two outer quartets for the crystal structure are not identical, and therefore 16 distinct $^{h3}J_{N1C6'}$ couplings were computed. Experimental $^{h3}J_{N1C6'}$ couplings of the Na^+-bound DNA quadruplex at 298 K were taken from a previous study.[54] Only six out of a possible eight $^{h3}J_{N1C6'}$ couplings were measured for the Na^+-bound DNA quadruplex.[54] The corresponding couplings in the K^+-bound DNA quadruplex have not been determined experimentally.

The computed $^{h3}J_{N1C6'}$ couplings are all negative in sign except for the G1*–G9 H-bond (0.04 Hz) in the outer quartet of the Na^+-coordinated DNA quadruplex (Table 5). The explanation for this positive $^{h3}J_{N1C6'}$ coupling observed for the G1*–G9 N1-H1···O6=C6 H-bond is presumably due to the exceptionally non-linear H···O=C angle (116°). Examination of the geometric dependencies of the computed $^{h3}J_{N1C6'}$ couplings (Figure 9a) shows that there is a reasonable correlation between the $^{h3}J_{N1C6'}$ couplings and the $\measuredangle$H···O=C values which were obtained from the G-quartet crystal structures with B3LYP/6-31G(d) geometry optimized hydrogen positions. In contrast, a much weaker correlation is observed between the $\measuredangle$N-H···O and $^{h3}J_{N1C6'}$ coupling constants (see Supporting Information). This observation corroborates DFT studies examining the N-H···O=C H-bond moiety in formamide dimers.[35,36] Here, a very weak dependence of $^{h3}J_{N1C6'}$ on the $\measuredangle$N-H···O in the range of 150–210° was found, whereas a substantial dependence of $^{h3}J_{N1C6'}$ on the $\measuredangle$H···O=C values in the range of 120–240° was calculated. There is a decrease in the size of the $|^{h3}J_{N1C6'}|$ couplings with decreasing $\measuredangle$H···O=C values, which can be explained by a reduced orbital overlap between the donor and acceptor groups in more non-linear $\measuredangle$H···O=C. Geometric considerations using a simple N-H···O=C-N model system which uses atomic and trigonal hybrid-type orbitals[36] showed that there is a $\cos^2$ dependence of $^{h3}J_{N1C6'}$ on the H···O=C angle. A linear regression between $\cos^2(\measuredangle$H···O=C) and $^{h3}J_{N1C6'}$ for the outer and inner quartets in both DNA quadruplexes yields:

$$^{h3}J_{N1C6'} = -2.43\cos^2(\theta) + 0.59\,\text{Hz} \quad (5)$$

where θ represents $\measuredangle$H···O=C. The standard deviation is 0.18 Hz and $r^2 = 0.78$.

Figure 9a shows that the sign of the coupling changes at an $\measuredangle$H···O=C value of 119.5°. Equation (5) only takes the $\measuredangle$H···O=C dependence of the $^{h3}J_{N1C6'}$ couplings into account and ignores other geometric factors such as the H-bond length (i.e., R_{N1O6}). A plot of $^{h3}J_{N1C6'}$ couplings (Figure 9b) versus R_{N1O6} shows no exponential correlation ($r^2 = 0.09$). This is partially due to the positive coupling for the G1*–G9 H-bond, as indicated by the much better correlation ($r^2 = 0.46$) obtained by excluding this point from the fit (Figure 9b). Although this observation suggests that this point is an outlier, the G1*–G9 $^{h3}J_{N1C6'}$ coupling corresponds well with the angular dependency (Figure 9a). The poor correlation observed for the $^{h3}J_{N1C6'}$ couplings versus R_{N1O6} contrasts the exponential correlation between experimentally observed $^{h3}J_{N1C6'}$ couplings and H-bond lengths in the B1 immunoglobulin binding domain of protein G.[17] However, as shown in Figure 9b, a plot of the data[17] for protein G over the R_{N1O6} range found in the G-quartets gives a much poorer correlation ($r^2 = 0.46$) than previously reported. Apparently, the wider spread of the H-bond lengths in protein G coupled with the more linear $\measuredangle$H···O=C and $\measuredangle$N-···O

Table 6. Computed chemical shifts in optimized G4-M^+ (M = Na, K) quartets and in G-quartets taken from the Na^+ and K^+ DNA quadruplexes with the hydrogen atom positions optimized using B3LYP/6-31G(d).

	^{1}H21[a]		^{1}H22[a]		^{15}N2[a]		^{15}N7[a]		^{1}H1[a]		^{15}N1[a]		^{13}C6[a]	
	Na^+	K^+	Na^+	K^+	Na^+	K^+	Na^+	K^+	Na^+	K^+	Na^+	K^+	Na^+	K^+
C_{4h}-symmetric quartet with an ion (Na^+, K^+) in the middle of the cavity, optimized with B3LYP/6-31+G(d)	9.5	8.0	4.3	4.3	106.6	103.6	277.2	180.5	11.3	10.3	176.4	175.1	166.7	165.6
outer quartet (donor guanine)														
1	12.6	12.0	3.6	3.5	106.8	106.2	277.1	283.2	11.5	12.2	176.5	177.7	163.2	163.4
9*	8.0	9.5	3.6	3.7	99.0	105.2	276.7	277.1	11.4	12.1	177.4	177.1	161.9	162.3
12	8.0	8.4	3.5	3.5	99.4	100.0	279.1	278.1	11.6	11.8	179.7	180.7	162.6	162.9
4*	10.5	9.8	3.6	3.6	104.0	102.9	281.3	275.9	11.6	12.2	177.2	178.4	163.2	162.2
inner quartet														
2	10.7	10.1	3.6	3.7	104.5	100.1	278.8	275.0	11.3	11.5	178.1	173.9	163.7	164.3
3*	8.7	9.5	3.6	3.7	100.9	99.9	277.3	278.4	11.4	12.4	178.1	173.1	161.7	162.8
11	9.6	10.6	3.5	3.7	101.8	103.3	278.1	278.5	12.0	12.0	177.2	176.2	153.5	164.7
10*	10.1	9.8	3.6	3.8	103.6	105.7	278.8	276.7	12.0	12.5	177.0	178.6	161.4	163.9
inner quartet														
3	9.3	9.9	3.7	3.7	100.6	101.8	277.2	280.9	11.1	11.7	176.8	177.3	160.2	165.3
11*	9.6	9.1	3.6	3.8	102.2	100.7	274.8	278.5	12.9	11.2	180.0	169.8	163.5	162.0
10	10.7	9.3	3.8	3.8	107.3	101.3	278.7	281.7	12.1	12.1	175.3	178.2	161.8	165.6
2*	10.0	8.6	3.7	3.9	104.3	99.5	278.0	277.8	12.1	11.8	179.5	171.5	162.4	161.6
outer quartet														
4	10.8	10.2	3.7	3.6	101.0	104.0	283.4	273.7	11.0	12.3	176.6	176.2	163.7	161.9
1*	13.2	10.0	3.6	3.6	106.8	102.8	281.4	279.0	11.5	12.7	175.5	174.7	164.2	164.2
9	7.9	9.6	4.0	3.9	99.8	105.7	275.3	279.5	11.9	12.2	176.3	175.8	160.8	162.0
12*	10.0	9.8	3.5	3.5	102.5	101.2	278.0	275.3	13.3	11.9	184.3	178.1	163.9	164.1
experimental[b]	8–11		6–8		79–84		229–240		11–12		140–150		161–163	

[a] Chemical shifts are in ppm. [b] Chemical shift ranges are taken from published data on the Na^+ DNA quadruplex.[54]

values gives rise to a stronger distance dependence of $^{h3}J_{N1C6'}$ couplings in proteins compared to the data presented for the G-quartets. These observations are supported by theoretical calculations that have shown that at substantially non-linear ∢H···O=C values the H-bond distance dependence of the $^{h3}J_{N1C6'}$ coupling is the weakest and the H···O=C angle dependence is the strongest.[36] As such, it appears that the presence of rather non-linear ∢H···O=C values in the G•G Hoogsteen base pairs is the principal geometric factor influencing the size of the calculated $^{h3}J_{N1C6'}$ couplings. The size of the $^{h3}J_{N1C6'}$ couplings in proteins is significantly larger compared with the $^{h3}J_{N1C6'}$ couplings computed in this study for G-quartets. As previously reported,[54] the ∢H···O=C values in protein G range between 137–172°, whereas in the G-quartets this range is 116–123°. As more linear ∢H···O=C values yield larger $|^{h3}J_{N1C6'}|$ couplings (Figure 9a), the larger $^{h3}J_{N1C6'}$ values observed in protein G can be partially attributed to the differences in the ∢H···O=C between protein G and the G-quartets. Barfield[36] noted that for coplanar formamide dimers the size of the $^{h3}J_{N1C6'}$ coupling is independent of the H···O=C-N dihedral angle. Since the guanine bases in the G-quartets are nearly coplanar, the $^{h3}J_{N1C6'}$ couplings are essentially independent of the H···O=C-N dihedral angle (data not shown).

Clearly, the calculated NMR parameters related to the N1-H1···O6=C6 H-bond in G-quartets are not well correlated with an *individual* geometric property, but depend on a *combination* of these structural features. Although limited by the data set size, a three-dimensional plot of the $^{h3}J_{N1C6'}$ couplings as a function of both the R_{N1O6} and ∢H···O=C shows that the couplings are correlated to both the R_{N1O6} and ∢H···O=C geometric properties (see Supporting Information). Similar dual correlations have been observed for *N*-methylacetamide,[33] protein–nucleotide models,[86] and formamide[35] dimers in which the size of *trans*-H-bond coupling is influenced by both distance and angular dependencies. Although it is feasible that the chemical character of the N1-H1···O6=C6 H-bond may play a role in influencing the relations between the NMR parameters and the H-bond geometry, this and previous studies[4,32,54] have shown that the chemical moiety of the H-bond has a minor effect on the size of the scalar couplings in nucleic acids.

The theoretical $^{h3}J_{N1C6'}$ couplings compare well with the experimental $^{h3}J_{N1C6'}$ couplings determined for the Na^+-bound DNA quadruplex (Figure 9a). There is no clear geometric dependency observed for the measured $^{h3}J_{N1C6'}$ couplings. This is presumably due to the dynamics of the solution structure averaging out any small ∢H···O=C and R_{N1O6} geometric influences on the magnitude of the couplings or genuine differences between the crystal versus solution structures. The inability to experimentally determine the $^{h3}J_{N1C6'}$ coupling size for the G1–G9* H-bond is probably due to its unusually bent ∢H···O=C which apparently decreases the absolute size of the coupling to the extent that it is unobservable in the NMR spectra.

The calculated ^{1}H1 and ^{13}C6 isotropic chemical shift values are in very good agreement with the experimental values (Table 6).[54] Neglecting different physicochemical conditions, the average difference between the theoretical and experimental (data taken at 298 K) results for the ^{1}H1 and ^{13}C6 chemical shifts are 0.6 and 1.4 ppm, respectively. Additionally, the theoretical ^{13}C chemical shifts for the C2,

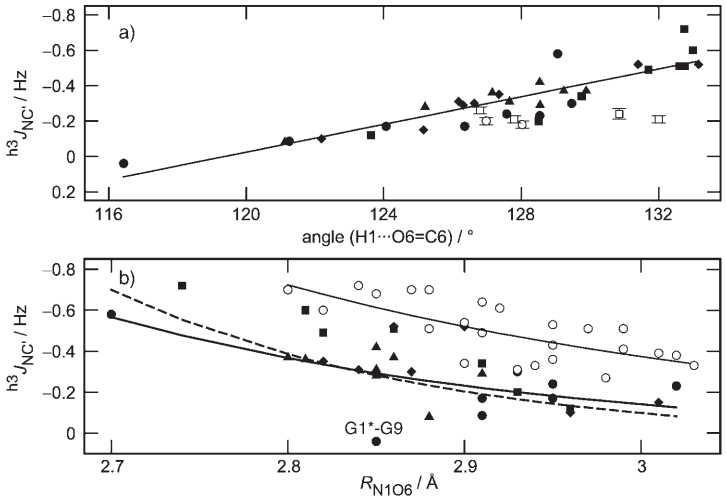

Figure 9. Correlations between $^{h3}J_{N1C6'}$ couplings and the a) ∢H···O=C and b) R_{N1O6} of the N1-H1···O6=C6 H-bond moiety in G-quartets. The theoretical couplings were calculated for G-quartet structures taken from the crystallographic data with the hydrogen atom positions optimized using B3LYP/6-31G(d). Computed data for the different G-quartets are represented by the same symbols as in Figure 7. The six experimental couplings determined previously[54] from the Na^+ DNA quadruplex (G12-G4*, G4*-G1, G2-G3*, G3-G11, G11-G10*, and G10*-G2 H-bonds) are represented by the corresponding open symbol. Open circles in b) represent $^{h3}J_{N1C6'}$ couplings determined for protein G.[17] The R_{N1O6} values are averaged over the three protein G crystal structures (1PGB, 1IGD, and 2IGD). The continuous line in a) corresponds to linear regression ($r^2=0.78$) using Eq. (5), whereas the curves b) represent the best-fit exponentials to the G-quartet theoretical data ($r^2=0.09$) and experimental data for protein G ($r^2=0.46$). The dashed line represents the exponential fit to the G-quartet data ($r^2=0.46$) that excludes the G1*–G9 H-bond $^{h3}J_{N1C6'}$ coupling (labeled).

C4, C5, and C8 atoms in the guanine base are also in very good agreement with the experimental values (data not shown). In contrast, all the calculated ^{15}N chemical shifts are generally overestimated by approximately 35 ppm (Table 6). The most likely explanation for this discrepancy is the uncertainties introduced from the indirect way that the ^{15}N referencing is determined. However, the possibility that the differences between the theoretical and experimental ^{15}N chemical shifts are not due to other factors such as the absence of interactions from solvent and other structural features cannot be currently excluded. Weak correlations are observed between the H-bond length and the isotropic chemical shifts of the donor nuclei of the N1-H1···O6=C6 H-bond, whereas much stronger correlations are observed between the R_{N2N7} of the N2-H2···N7 H-bond and the $^{15}N2$ and $^{1}H2$ chemical shifts (see Supporting Information). An examination of the dependencies of the various H-bond angles on the ^{1}H and ^{15}N chemical shifts shows no correlation. These results support the observed weaker correlations between the scalar couplings associated with the N1-H1···O6=C6 H-bond and the H-bond geometric parameters.

Conclusion

Hartree–Fock and density functional theory calculations were used to examine the energetic preferences of Na^+, Li^+, and K^+ ions in C_{4h} and S_4 symmetric G-quartets. The presence of a monovalent ion in the center of the G-quartet led to the contraction of the G-quartet O6–O6 distance. This effect was largest for the smallest ion, thus showing that the contraction of the G-quartet facilitates the optimal coordination of the monovalent ion with the O6 atoms of the guanine bases. The results for the G4-M^+-G4 model showed that at quartet–quartet distances observed in the DNA quadruplex crystal structures, the smaller Na^+ and Li^+ ions have two shallow minima located at 0.55 and 0.95 Å outside the plane of the G-quartet, respectively. The larger K^+ ion has a minimum centered between successive G-quartets. At increasing quartet–quartet distances the Na^+ and Li^+ ions converged to a position coplanar with the G-quartet, whereas the optimal K^+ ion position converged to a location just outside the G-quartet. Apparently at shorter quartet–quartet distances the Na^+ and Li^+ ions are weakly attracted to the second G-quartet and therefore do not favor a coplanar position with the G-quartet. Increasing the quartet–quartet distance reduces this weak attraction to zero and the Na^+ and Li^+ ions shift to an energetically favored coplanar position. The attraction of the ion to both G-quartets at quartet–quartet distances observed in DNA quadruplex structures may facilitate the transport of the ions through the DNA quadruplex central channel. The K^+ ion never energetically favored a coplanar position at any quartet–quartet distance examined. Presumably in a dynamic system, the G-quartets expand and contract to accommodate the movement of the K^+ ion through the G-quartet. Evidence for this comes from the differences in the geometries of the calculated coplanar K^+ G-quartet and the crystallographic data. In the crystal structure, the K^+ ions are located between the planes of two G-quartets with an O6–O6 distance of ~4.5 Å, whereas a larger O6–O6 distance of 5.1–5.2 Å is observed at the HF/6-31G(d) and B3LYP/6-31+G(d) levels of theory for the C_{4h}-symmetric coplanar K^+ G-quartet. Thus, the G-quartet needs to expand from the geometry it adopts in the DNA quadruplex to allow passage of the K^+ ion through the central cavity.

To allow movement of ions through the central channel of the DNA quadruplexes, the ions must overcome the energy barriers separating the minima. As the energy barriers are rather low for the Na^+ and Li^+ models, vibrational and thermodynamic effects will likely be able to overcome these barriers. The energy barriers separating the minima become significantly larger with increasing quartet–quartet distances for the Na^+ and Li^+ models, thus suggesting that the quartet–quartet distances found in DNA quadruplexes are near optimal for the flow of the Na^+ and Li^+ ions through the central pore of the DNA quadruplex. The K^+ ion models showed much larger energy barriers for the movement of the ion through the central cavity of the G-quartets. Consequently, the K^+ ions will not be able to move as easily through the central channel of the DNA quadruplex. The

possible expansion and contraction of the G-quartets may facilitate the lowering of these energy barriers. The results herein support the observation that the ion movement through DNA quadruplexes for the smaller Na^+ ion is three-orders of magnitude faster than for the larger NH_4^+ ion (mimics the size of K^+).[53,87]

Theoretical calculations of spin-spin couplings and isotropic chemical shifts in the N1-H1···O6=C6 and N2-H2···N7 H-bonding regions of G-quartets extracted from the K^+- and Na^+-coordinated Oxy-1.5 DNA quadruplexes and the C_{4h} symmetric structures were performed. The results showed that the sizes of the *trans*-H-bond couplings were influenced primarily by the geometry of the H-bond and only slightly by the presence of the monovalent ion. The calculated $^{h2}J_{N2N7}$ couplings decrease exponentially with increasing N2-H2···N7 H-bond length. The $^{h3}J_{N1C6'}$ couplings are shown to be dependent on both the $R_{N\cdots O}$ and $\measuredangle$H···O=C geometric properties. An increasing $R_{N\cdots O}$ value leads to a decrease in the size of the $^{h3}J_{N1C6'}$ coupling, whereas a linear H···O=C angle gives the strongest coupling. At more bent $\measuredangle$H···O=C values the angular dependency is the principal geometric property influencing the magnitude of the $^{h3}J_{N1C6'}$ couplings. The computed *trans*-H-bond couplings are shown to correlate with the experimentally determined couplings however, the experimental values do not show such strong geometric dependencies. A strong correlation was found between the $^{h2}J_{N2N7}$ and the donor amide proton isotropic chemical shift. Conversely, a weak correlation between the $^{h3}J_{N1C6'}$ and the imino proton isotropic chemical shift was observed. This weak correlation counters previous results in which a strong correlation between the $^{h3}J_{N1C6'}$ couplings and amide proton chemical shifts was measured in proteins,[15] and indicates that the imino chemical shift in the G-quartets is influenced by other factors not directly related to the H-bond moiety. The results show that the distance, rather than angle, of the N2-H2···N7 H-bond can be characterized by strong correlations to both the isotropic chemical shifts of the donor group atoms and the $^{h2}J_{N2N7}$ couplings. In contrast, the NMR parameters for the N1-H1···O6=C6 H-bond show weaker correlations to single geometric parameters related to this H-bond. This observation indicates that for a full interpretation of the $^{h3}J_{N1C6'}$ couplings dependency on the geometry of the H-bond a combined distance–angle relation is required. The results provide the framework for further theoretical characterization of the ion dependent stability and structure of the H-bonding network of the G-quartet motif.

Acknowledgements

T.v.M. gratefully acknowledges support from the Royal Society via the University Research Fellowship scheme, as well as support from the Engineering and Physical Sciences Research Council (through grants GR/R63196/01 and GR/S06233/01). The authors thank Professors Juli Feigon and Stephan Grzesiek for their support. We also thank Dr. Ad Bax for the permission to use the published $^{h3}J_{NC'}$ data in Figure 9.

[1] G. A. Jeffrey, W. Saenger, *Hydrogen Bonding in Biological Structures*, Springer, New York, **1991**.
[2] A. Fersht, *Structure and Mechanism in Protein Science*, W. H. Freeman, New York, **1998**.
[3] A. J. Dingley, S. Grzesiek, *J. Am. Chem. Soc.* **1998**, *120*, 8293–8297.
[4] A. J. Dingley, J. E. Masse, R. D. Peterson, M. Barfield, J. Feigon, S. Grzesiek, *J. Am. Chem. Soc.* **1999**, *121*, 6019–6027.
[5] J. Wöhnert, A. J. Dingley, M. Stoldt, M. Gorlach, S. Grzesiek, L. R. Brown, *Nucleic Acids Res.* **1999**, *27*, 3104–3110.
[6] K. Pervushin, A. Ono, C. Fernandez, T. Szyperski, M. Kainosho, K. Wuthrich, *Proc. Natl. Acad. Sci. USA* **1998**, *95*, 14147–14151.
[7] K. Pervushin, C. Fernandez, R. Riek, A. Ono, M. Kainosho, K. Wuthrich, *J. Biomol. NMR* **2000**, *16*, 39–46.
[8] A. Liu, A. Majumdar, W. Hu, A. Kettani, E. Skripkin, D. J. Patel, *J. Am. Chem. Soc.* **2000**, *122*, 3206-3210.
[9] A. Majumdar, A. Kettani, E. Skripkin, D. J. Patel, *J. Biomol. NMR* **1999**, *15*, 207–211.
[10] A. Majumdar, A. Kettani, E. Skripkin, *J. Biomol. NMR* **1999**, *14*, 67–70.
[11] A. Majumdar, A. Kettani, E. Skripkin, D. J. Patel, *J. Biomol. NMR* **2001**, *19*, 103–113.
[12] B. Luy, J. P. Marino, *J. Am. Chem. Soc.* **2000**, *122*, 8095–8096.
[13] B. Luy, U. Richter, E. S. DeJong, O. W. Sorensen, J. P. Marino, *J. Biomol. NMR* **2002**, *24*, 133–142.
[14] D. P. Giedroc, P. V. Cornish, M. Hennig, *J. Am. Chem. Soc.* **2003**, *125*, 4676–4677.
[15] F. Cordier, S. Grzesiek, *J. Am. Chem. Soc.* **1999**, *121*, 1601–1602.
[16] F. Cordier, M. Rogowski, S. Grzesiek, A. Bax, *J. Magn. Reson.* **1999**, *140*, 510–512.
[17] G. Cornilescu, B. E. Ramirez, M. K. Frank, G. M. Clore, A. M. Gronenborn, A. Bax, *J. Am. Chem. Soc.* **1999**, *121*, 6275–6279.
[18] G. Cornilescu, J.-S. Hu, A. Bax, *J. Am. Chem. Soc.* **1999**, *121*, 2949–2950.
[19] A. Meissner, O. W. Sorensen, *J. Magn. Reson.* **2000**, *143*, 431–434.
[20] A. Meissner, O. W. Sorensen, *J. Magn. Reson.* **2000**, *143*, 387–390.
[21] F. Cordier, M. Barfield, S. Grzesiek, *J. Am. Chem. Soc.* **2003**, *125*, 15750–15751.
[22] F. Löhr, S. G. Mayhew, H. Rüterjans, *J. Am. Chem. Soc.* **2000**, *122*, 9289–9295.
[23] M. Mishima, M. Hatanaka, S. Yokoyama, T. Ikegami, M. Wälchli, Y. Ito, M. Shirakawa, *J. Am. Chem. Soc.* **2000**, *122*, 5883–5884.
[24] S. Grzesiek, F. Cordier, A. J. Dingley, *Methods Enzymol.* **2001**, *338*, 111–133.
[25] N. Juranic, M. C. Moncrieffe, V. A. Likic, F. G. Prendergast, S. Macura, *J. Am. Chem. Soc.* **2002**, *124*, 14221–14226.
[26] F. Cordier, S. Grzesiek, *Biochemistry* **2004**, *43*, 11295–11301.
[27] F. Cordier, S. Grzesiek, *J. Mol. Biol.* **2002**, *317*, 739–752.
[28] F. Cordier, C. Wang, S. Grzesiek, L. K. Nicholson, *J. Mol. Biol.* **2000**, *304*, 497–505.
[29] V. A. Jaravine, A. T. Alexandrescu, S. Grzesiek, *Protein Sci.* **2001**, *10*, 943–950.
[30] V. A. Jaravine, F. Cordier, S. Grzesiek, *J. Biomol. NMR* **2004**, *29*, 309–318.
[31] F. M. Assadi-Porter, F. Abildgaard, H. Blad, J. L. Markley, *J. Biol. Chem.* **2003**, *278*, 31331–31339.
[32] M. Barfield, A. J. Dingley, J. Feigon, S. Grzesiek, *J. Am. Chem. Soc.* **2001**, *123*, 4014–4022.
[33] C. Scheurer, R. Brüschweiler, *J. Am. Chem. Soc.* **1999**, *121*, 8661–8662.
[34] W. D. Arnold, E. Oldfield, *J. Am. Chem. Soc.* **2000**, *122*, 12835–12841.
[35] A. Bagno, *Chem. Eur. J.* **2000**, *6*, 2925–2930.
[36] M. Barfield, *J. Am. Chem. Soc.* **2002**, *124*, 4158–4168.
[37] S. J. Wilkens, W. M. Westler, J. L. Markley, F. Weinhold, *J. Am. Chem. Soc.* **2001**, *123*, 12026–12036.
[38] J. E. Peralta, G. E. Scuseria, J. R. Cheeseman, M. J. Frisch, *Chem. Phys. Lett.* **2003**, *375*, 452–458.

[39] T. Tuttle, E. Kraka, A. Wu, D. Cremer, *J. Am. Chem. Soc.* **2004**, *126*, 5093–5107.
[40] P. Salvador, N. Kobko, R. Wieczorek, J. J. Dannenberg, *J. Am. Chem. Soc.* **2004**, *126*, 14190–14197.
[41] N. F. Ramsay, *Phys. Rev.* **1953**, *91*, 303–307.
[42] S. Neidle, G. N. Parkinson, *Curr. Opin. Struct. Biol.* **2003**, *13*, 275–283.
[43] H. Han, L. H. Hurley, *Trends Pharmacol. Sci.* **2000**, *21*, 136–142.
[44] W. I. Sundquist, A. Klug, *Nature* **1989**, *342*, 825–829.
[45] K. Phillips, Z. Dauter, A. I. Murchie, D. M. Lilley, B. Luisi, *J. Mol. Biol.* **1997**, *273*, 171–182.
[46] N. V. Hud, F. W. Smith, F. A. Anet, J. Feigon, *Biochemistry* **1996**, *35*, 15383–15390.
[47] W. S. Ross, C. C. Hardin, *J. Am. Chem. Soc.* **1994**, *116*, 6070–6080.
[48] J. Gu, J. Leszczynski, M. Bansal, *Chem. Phys. Lett.* **1999**, *311*, 209–214.
[49] J. Gu, J. Leszczynski, *J. Phys. Chem. A* **2000**, *104*, 6308–6313.
[50] G. Louit, A. Hocquet, M. Ghomi, M. Meyer, J. Sühnel, *Phys. Chem. Commun.* **2002**, *5*, 94–98.
[51] M. Meyer, T. Steinke, M. Brandl, J. Sühnel, *J. Comput. Chem.* **2001**, *22*, 109–124.
[52] M. Meyer, M. Brandl, J. Sühnel, *J. Phys. Chem. A* **2001**, *105*, 8223–8225.
[53] H. Deng, W. H. Braunlin, *J. Mol. Biol.* **1996**, *255*, 476–483.
[54] A. J. Dingley, J. E. Masse, J. Feigon, S. Grzesiek, *J. Biomol. NMR* **2000**, *16*, 279–289.
[55] P. Schultze, F. W. Smith, J. Feigon, *Structure* **1994**, *2*, 221–233.
[56] P. Schultze, N. V. Hud, F. W. Smith, J. Feigon, *Nucleic Acids Res.* **1999**, *27*, 3018–3028.
[57] F. W. Smith, J. Feigon, *Nature* **1992**, *356*, 164–168.
[58] M. P. Horvath, S. C. Schultz, *J. Mol. Biol.* **2001**, *310*, 367–377.
[59] S. Haider, G. N. Parkinson, S. Neidle, *J. Mol. Biol.* **2002**, *320*, 189–200.
[60] NWChem, Version 4.5, High Performance Computational Chemistry Group, Pacific Northwest National Laboratory, Richland WA, **2003**.
[61] A. D. Becke, *Phys. Rev. A* **1988**, *38*, 3098–3100.
[62] C. Lee, W. Yang, R. G. Parr, *Phys. Rev. B* **1988**, *37*, 785–789.
[63] A. D. Becke, *J. Chem. Phys.* **1993**, *98*, 5648–5652.
[64] A. D. Becke, *J. Chem. Phys.* **1997**, *107*, 8554–8560.
[65] Gaussian 03, Revision B.04, M. J. Frisch, G. W. Trucks, H. B. Schlegel, G. E. Scuseria, M. A. Robb, J. R. Cheeseman, J. A. Montgomery, Jr., T. Vreven, K. N. Kudin, J. C. Burant, J. M. Millam, S. S. Iyengar, J. Tomasi, V. Barone, B. Mennucci, M. Cossi, G. Scalmani, N. Rega, G. A. Petersson, H. Nakatsuji, M. Hada, M. Ehara, K. Toyota, R. Fukuda, J. Hasegawa, M. Ishida, T. Nakajima, Y. Honda, O. Kitao, H. Nakai, M. Klene, X. Li, J. E. Knox, H. P. Hratchian, J. B. Cross, V. Bakken, C. Adamo, J. Jaramillo, R. Gomperts, R. E. Stratmann, O. Yazyev, A. J. Austin, R. Cammi, C. Pomelli, J. W. Ochterski, P. Y. Ayala, K. Morokuma, G. A. Voth, P. Salvador, J. J. Dannenberg, V. G. Zakrzewski, S. Dapprich, A. D. Daniels, M. C. Strain, O. Farkas, D. K. Malick, A. D. Rabuck, K. Raghavachari, J. B. Foresman, J. V. Ortiz, Q. Cui, A. G. Baboul, S. Clifford, J. Cioslowski, B. B. Stefanov, G. Liu, A. Liashenko, P. Piskorz, I. Komaromi, R. L. Martin, D. J. Fox, T. Keith, M. A. Al-Laham, C. Y. Peng, A. Nanayakkara, M. Challacombe, P. M. W. Gill, B. Johnson, W. Chen, M. W. Wong, C. Gonzalez, J. A. Pople, Gaussian, Inc., Wallingford CT, **2004**.
[66] S. F. Boys, F. Bernardi, *Mol. Phys.* **1970**, *19*, 553–557.
[67] P. H. Smit, F. B. Derissen, F. B. van Duijneveldt, *J. Chem. Phys.* **1978**, *69*, 4241–4244.
[68] P. Salvador, J. J. Dannenberg, *J. Phys. Chem. B* **2004**, *108*, 15370–15375.
[69] R. Ditchfield, *Mol. Phys.* **1974**, *27*, 789–807.
[70] K. Wolinski, J. F. Hinton, P. Pulay, *J. Am. Chem. Soc.* **1990**, *112*, 8251–8260.
[71] W. Kutzelnigg, U. Fleischer, M. Schindler, *NMR basic principles and progress*, Springer, Berlin, **1990**, pp. 165–262.
[72] M. Alei, Jr., A. E. Florin, W. M. Litchman, J. F. O'Brien, *J. Phys. Chem.* **1971**, *75*, 932–938.
[73] W. M. Litchman, M. Alei, Jr., A. E. Florin, *J. Chem. Phys.* **1969**, *50*, 1031–1032.
[74] M. Witanowski, L. Stefaniak, G. A. Webb, *Ann. Rep. NMR Spectrosc.* **1993**, *25*, 88.
[75] J. Gu, J. Leszczynski, *J. Phys. Chem. A* **2003**, *107*, 9447–9455.
[76] B. J. Lynch, Y. Zhao, D. G. Truhlar, *J. Phys. Chem. A* **2003**, *107*, 1384–1388.
[77] M. Meyer, A. Hocquet, J. Sühnel, *J. Comput. Chem.* **2005**, *26*, 352–364.
[78] J. H. Ippel, S. S. Wijmenga, R. de Jong, H. A. Heus, C. W. Hilbers, E. de Vroom, G. A. van der Marel, V. A. van Boom, *Magn. Reson. Chem.* **1996**, *34*, S156-S176.
[79] L. Zidek, H. Wu, J. Feigon, V. Sklenar, *J. Biomol. NMR* **2001**, *21*, 153–160.
[80] M. L. Munzarova, V. Sklenar, *J. Am. Chem. Soc.* **2003**, *125*, 3649–3658.
[81] M. L. Munzarova, V. Sklenar, *J. Am. Chem. Soc.* **2002**, *124*, 10666–10667.
[82] V. Sychrovsky, J. Sponer, P. Hobza, *J. Am. Chem. Soc.* **2004**, *126*, 663–672.
[83] R. S. Mulliken, C. A. Rieke, D. Orloff, H. Orloff, *J. Chem. Phys.* **1949**, *17*, 1248–1267.
[84] P. R. Markwick, R. Sprangers, M. Sattler, *J. Am. Chem. Soc.* **2003**, *125*, 644–645.
[85] H. Benedict, I. G. Shenderovich, O. L. Malkina, V. G. Malkin, G. S. Denisov, N. S. Golubev, H.-H. Limbach, *J. Am. Chem. Soc.* **2000**, *122*, 1979–1988.
[86] J. Czernek, R. Bruschweiler, *J. Am. Chem. Soc.* **2001**, *123*, 11079–11080.
[87] N. V. Hud, P. Schultze, V. Sklenar, J. Feigon, *J. Mol. Biol.* **1999**, *285*, 233–243.

Received: February 22, 2005
Published online: July 29, 2005

